

ISRN LUTMDN/TMHP-17/5391-SE  
ISSN 0282-1990

# Transient model of a driven compressor

---

**LUND UNIVERSITY**

Rasmus Johnsson  
Sebastian Norén

Thesis for the Degree of Master of Science  
Division of Thermal Power Engineering  
Department of Energy Science  
Lund Institute of Technology | Lund University





## Transient model of a driven compressor



# Transient model of a driven compressor

by Rasmus Johnsson and Sebastian Norén



**LUND**  
UNIVERSITY

Thesis for the Degree of Master of Science  
Thesis advisors: Assoc. Prof. Marcus Thern, Anna Sjunnesson



This thesis for the degree of Master of Science in Engineering has been conducted at the Division of Thermal Power Engineering, Department of Energy Sciences, LTH – Lund University and at Siemens Industrial Turbomachinery AB. Supervisor at Siemens Industrial Turbomachinery AB: Anna Sjunnesson; supervisor at LU-LTH: Assoc. Prof. Marcus Thern; examiner at LU-LTH: Prof. Magnus Genrup.

© Rasmus Johnsson and Sebastian Norén 2017

Division of Thermal Power Engineering, Department of Energy Science  
Box 118, 221 00 Lund  
[www.energy.lth.se](http://www.energy.lth.se)

ISSN: <0282-1990>

Printed in Sweden by Media-Tryck, Lund University, Lund 2017



*"Education is what remains after one has forgotten what one has learned in school"*  
- Albert Einstein



# Abstract

Industrial gas turbines are widely used in different applications. These can be divided into two main categories; power generation (PG) and mechanical drive (MD). To be able to predict the performance of the system, Siemens has during the years developed simulation models for both steady state and transient operation. These models are mainly designed for PG, so there is a need for new MD models. An MD model includes a gas turbine, a driven component, in this case a compressor, and auxiliary systems which ensures stable operation and avoid rotating stall and surge in the compressor.

The purpose of this thesis is to develop a transient model of a driven compressor based on characteristics and connect it with the existing dynamic gas turbine model of the Siemens Gas Turbine 750 (SGT-750) in Dymola. Auxiliary systems are developed for both the compressor system and for the compressor train in order to reflect the reality and get reliable simulation results. An analysis is performed to study the behaviour of the compressor train when controller and physical parameters are changed.

The developed compressor model is based on the existing basic compressor model developed by Siemens. Compressor maps from the reference project El-Encino were implemented in the model and were verified against data sheets and the model was then connected to the existing SGT-750 model in Dymola. New controllers were developed to ensure reliable operation of the compressor train and the complete model was then tuned in and verified towards measured data from two different sites with the SGT-700 as the driving component. Different cases were simulated to assure stable operation for varying starting conditions and to study the behaviour of the compressor train.

The verification shows that the developed model corresponds to reality with deviations within the approved area, with regard of the limitations of the project. The model now makes it possible to study the gas turbine behaviour in an MD application with the SGT-750 as the driving component. The configuration of the gas turbine control system makes it possible to use it in different applications with different gas turbines, both for PG and MD. The behaviour analysis shows that a lower fuel ramp during start-up increases the stability of the compressor train. It also indicates that the power turbine acceleration controller could be redundant for certain cases but further analysis is needed in the matter. Due to the focus of the project and limitations in Dymola, more work is needed to ensure accuracy of all parameter values. There are improvement opportunities in the program's basic thermodynamic functions, which is a part of the future work.

**Keywords:** gas turbine, modelling, Dymola, SGT-750, mechanical drive, compressor train, thermodynamics, performance.

# Sammanfattning

Industriella gasturbiner används i många olika applikationer och tillämpningar. Dessa kan delas in i två huvudkategorier; Kraftgenerering (PG) och mekanisk drift (MD). För att kunna förutsäga systemens prestanda har Siemens genom åren utvecklat simuleringsmodeller för både *steady state* och transienta förlopp. Dessa modeller är huvudsakligen avsedda för PG, så det finns ett behov av nya MD-modeller. En MD-modell innehåller vanligtvis en gasturbin, den drivna komponenten, i detta fall en kompressor, samt hjälpsystem. Hjälpsystemen till modellen ska säkerställa stabil drift och undvika *Rotating stall* och *Surge* i kompressorn.

I detta examensarbete utvecklas en transient modell av en driven kompressor baserad på karaktäristik, som sammankopplas med den befintliga dynamiska gasturbinmodellen för Siemens Gas Turbine 750 (SGT-750) i Dymola. Hjälpsystem utvecklas för både kompressorsystemet och kompressortåget för att återspegla verkligheten och erhålla pålitliga simuleringsresultat. En analys utförs för att se hur kompressortåget svarar på ändringar av fysiska parametrar och parametrar i kontrollsystemet.

Kompressormodellen som utvecklas baseras på den befintliga baskompressormodellen utvecklad av Siemens. Kompressorkartor från referensprojektet El-Encino implementerades i modellen som därefter verifierades med hjälp av datablad och sammankopplades med den befintliga SGT-750 modellen i Dymola. Nya regulatorer utvecklades för att få tillförlitliga simuleringar av kompressortåget, den slutliga modellen trimmades sedan in och verifierades mot uppmätta data från två olika siter med SGT-700 som den drivande komponenten. Olika fall simulerades för att säkerställa stabil drift vid olika startförhållanden och för att studera beteendet hos kompressortåget.

Verifieringen visar att modellen motsvarar verkligheten med avvikelser inom ett godkänt område, med tanke på begränsningarna i projektet. Modellen gör det möjligt att studera gasturbinens beteende i en MD-applikation med SGT-750 som den drivande komponenten. Styrsystemets utformning gör det möjligt att använda det i andra applikationer och med andra gasturbiner, både för PG och MD. Beteendeanalysen visar att en lägre bränsleramp ger en stabilare start av kompressortåget. Den indikerar också att regulatorn som kontrollerar accelerationen av kraftturbinen är överflödigt i vissa fall. Dock bör detta analyseras vidare. På grund av arbetets avgränsningar samt begränsningar i Dymola behövs mer arbete för att kunna säkerställa noggrannheten av alla parametervärden. Förbättringsmöjligheter finns i programmets grundläggande termodynamiska funktioner vilka bör utvecklas ytterligare.

**Nyckelord:** gasturbin, modellering, Dymola, SGT-750, mekanisk drift, kompressortåg, termodynamik, prestanda.

## Acknowledgements

There are many people that have made this project possible, both at Siemens Industrial Turbomachinery AB (SIT) and at Lund University (LU). If all is to be mentioned the list would be very long.

Our biggest gratitude goes to Anna Sjunnesson, our supervisor at SIT. She has helped us from the first day and led us through the whole project. It has been an honour to be guided by her knowledge and experience, when meeting both silly and complex challenges.

We would like to thank the department manager Lennart Näs for giving us the opportunity to be a part of the performance department, and including us in the everyday work, Dr. Klas Jonshagen for his patient and understandable way of explaining complex thermodynamic problems.

We would also like to thank the whole performance department for their help and guidance throughout the project and for making us feel welcome at Siemens.

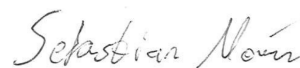
Many thanks to Prof. Magnus Genrup, who first introduced us to the world of turbines and created the opportunity to write this master thesis at SIT. We also want to thank our supervisor at LU, Assoc. Prof. Marcus Thern, for his guidance throughout the project. Our gratitude also goes to all employees at LU that have given us the knowledge needed in this project and in our future life as Mechanical Engineers.

Last but not least, thanks to our families and loved ones for all the support during the years!



---

Rasmus Johnsson  
Finspång 2017-06-12



---

Sebastian Norén  
Finspång 2017-06-12

# Nomenclature

| Latin symbols | Unit                                | Description                               |
|---------------|-------------------------------------|---|
| $A$           | $[\text{m}^2]$                      | Area                                      |
| $C$           | $[\text{m s}^{-1}]$                 | Velocity                                  |
| $c_\theta$    | $[\text{m s}^{-1}]$                 | Tangential speed                          |
| $c_p$         | $[\text{J kg}^{-1} \text{K}^{-1}]$  | Specific heat capacity, constant pressure |
| $c_v$         | $[\text{J kg}^{-1} \text{K}^{-1}]$  | Specific heat capacity, constant volume   |
| $D$           | $[\text{m}]$                        | Diameter                                  |
| $E$           | $[\text{kJ}]$                       | Energy                                    |
| $H$           | $[\text{J}]$                        | Enthalpy                                  |
| $h$           | $[\text{J kg}^{-1}]$                | Specific enthalpy                         |
| $J$           | $[\text{kg m}^2]$                   | Rotational inertia                        |
| $M$           | $[\text{kg mol}^{-1}]$              | Molar mass                                |
| $m$           | $[\text{kg}]$                       | Mass                                      |
| $\dot{m}$     | $[\text{kg s}^{-1}]$                | Mass flow                                 |
| $N$           | $[\text{rpm}]$                      | Rotational speed                          |
| $n$           | $[-]$                               | Number of inlet guide vanes               |
| $n_p$         | $[-]$                               | Number of purges required                 |
| $P$           | $[\text{W}]$                        | Power                                     |
| $p$           | $[\text{bar}]$                      | Pressure                                  |
| $Q$           | $[\text{J}]$                        | Heat                                      |
| $\dot{Q}$     | $[\text{kJ s}^{-1}]$                | Heat flow                                 |
| $R$           | $[\text{J kg}^{-1} \text{K}^{-1}]$  | Gas constant                              |
| $\bar{R}$     | $[\text{J mol}^{-1} \text{K}^{-1}]$ | The universal gas constant                |
| $r$           | $[\text{m}]$                        | Radius                                    |
| $s$           | $[\text{J kg}^{-1} \text{K}^{-1}]$  | Specific entropy                          |
| $T$           | $[\text{K}]$                        | Temperature                               |
| $U$           | $[\text{J}]$                        | Internal energy                           |

|                        | Unit                               | Description                                  |
|------------------------|------------------------------------|--|
| $u$                    | [J kg <sup>-1</sup> ]              | Specific internal energy                     |
| $V_w$                  | [m s <sup>-1</sup> ]               | Tangential velocity                          |
| $V_{GT}$               | [m <sup>3</sup> ]                  | Volume of the gas turbine                    |
| $V_{purgeExsys}$       | [m <sup>3</sup> ]                  | Volume of the exhaust system                 |
| $\dot{V}_{purgeExsys}$ | [m <sup>3</sup> s <sup>-1</sup> ]  | Air flow through exhaust system during purge |
| $\dot{V}_{purgeGT}$    | [m <sup>3</sup> s <sup>-1</sup> ]  | Air flow through gas turbine during purge    |
| $v$                    | [m <sup>3</sup> kg <sup>-1</sup> ] | Specific volume                              |
| $W$                    | [J]                                | Work   |
| $Z$                    | [m <sup>3</sup> s <sup>-1</sup> ]  | Compressibility                              |

| <b>Greek symbols</b> | Unit                   | Description                   |
|----------------------|------------------------|-------------------------------|
| $\gamma$             | [-]                    | Ratio between $c_p$ and $c_v$ |
| $\Delta$             | [-]                    | Difference                    |
| $\eta$               | [-]                    | Efficiency                    |
| $\rho$               | [kg m <sup>-3</sup> ]  | Density                       |
| $\sigma$             | [-]                    | Slip factor                   |
| $\tau$               | [N m]                  | Torque                        |
| $\psi$               | [-]                    | Power input factor            |
| $\Omega$             | [rad s <sup>-1</sup> ] | Angular velocity              |



# Contents

|   |          |
|---|----------|
| Abstract . . . . .  | i        |
| Sammanfattning . . . . .  | ii       |
| Acknowledgements . . . . .                                      | iii      |
| Nomenclature . . . . .  | iv       |
| <b>1 Introduction</b>   | <b>1</b> |
| 1.1 Background . . . . .  | 1        |
| 1.2 Objectives . . . . .  | 2        |
| 1.2.1 Problem definition . . . . .                              | 2        |
| 1.3 Limitations . . . . .                                       | 2        |
| 1.4 Method . . . . .  | 3        |
| 1.5 Tools . . . . .   | 4        |
| <b>2 Theory</b>   | <b>5</b> |
| 2.1 System description . . . . .                                | 5        |
| 2.1.1 Mechanical Drive . . . . .                                | 5        |
| 2.1.2 Compressor system . . . . .                               | 5        |
| 2.2 Compressor . . . . .  | 6        |
| 2.3 Centrifugal compressor . . . . .                            | 7        |
| 2.4 Energy and mass balance . . . . .                           | 7        |
| 2.5 Ideal gas model . . . . .                                   | 9        |
| 2.6 The momentum equation and the Euler work equation . . . . . | 10       |
| 2.7 Work done . . . . .   | 12       |
| 2.8 Compressor characteristics . . . . .                        | 13       |
| 2.9 Rotating stall and surge . . . . .                          | 17       |
| 2.10 Polytropic efficiency using the sT-method . . . . .        | 18       |
| 2.11 Gas turbine . . . . .                                      | 19       |
| 2.12 Heat transfer . . . . .                                    | 21       |
| 2.13 System control . . . . .                                   | 22       |
| 2.13.1 Anti-surge control . . . . .                             | 23       |
| 2.13.2 PID-controller . . . . .                                 | 23       |
| 2.14 Start-up sequence . . . . .                                | 25       |
| 2.15 Purge . . . . .  | 26       |
| 2.16 Natural gas . . . . .                                      | 27       |
| 2.17 El-Encino . . . . .  | 27       |
| 2.17.1 SGT-750 . . . . .  | 28       |

|          |  |           |
|----------|--|-----------|
| 2.17.2   | STC-SV   | 28        |
| 2.18     | Tools  | 28        |
| 2.18.1   | Dymola   | 28        |
| 2.18.2   | SVN/GITLab   | 29        |
| 2.18.3   | STA-RMS  | 29        |
| 2.18.4   | WebPlotDigitizer   | 29        |
| 2.18.5   | VLE Flash  | 29        |
| <b>3</b> | <b>Methodology</b>   | <b>31</b> |
| 3.1      | Literature study   | 31        |
| 3.2      | Dymola model of compressor system                                  | 32        |
| 3.2.1    | Compressor   | 32        |
| 3.2.1.1  | Basic Model  | 33        |
| 3.2.1.2  | Characteristics  | 33        |
| 3.2.2    | Medium   | 35        |
| 3.2.3    | Compressibility  | 35        |
| 3.2.4    | Anti-surge loop  | 36        |
| 3.2.4.1  | Control valve  | 36        |
| 3.2.4.2  | Control system   | 37        |
| 3.2.5    | Check valve  | 38        |
| 3.2.6    | Cooler   | 38        |
| 3.2.7    | Source, Sink and Volumes   | 39        |
| 3.2.8    | Ideal gas model  | 39        |
| 3.3      | Dymola model of gas turbine control system                         | 39        |
| 3.3.1    | Starter motor  | 41        |
| 3.3.2    | Start controller - STC   | 41        |
| 3.3.3    | Gas generator speed limiter - NGGL                                 | 41        |
| 3.3.4    | Power turbine acceleration controller - PAC                        | 41        |
| 3.3.5    | Frequency and load controller/Speed controller - FLC/SC            | 42        |
| 3.3.6    | Mass flow controller - MFC   | 42        |
| 3.3.7    | Exhaust temperature limiter - T0800L                               | 43        |
| 3.3.8    | Load loss detection - LLD  | 43        |
| 3.3.9    | Gas generator acceleration control - GAC                           | 44        |
| 3.3.10   | Flame sustain control - FSC  | 44        |
| 3.3.11   | Gas generator deceleration control - GDC                           | 44        |
| 3.3.12   | Bleed valve controller - BVC                                       | 45        |
| 3.4      | Implementation - Connecting the compressor system with the SGT-750 | 45        |
| <b>4</b> | <b>Verification and analysis</b>                                   | <b>47</b> |
| 4.1      | Verification of the compressor system                              | 47        |
| 4.1.1    | Compressor verification  | 48        |
| 4.1.2    | The ideal gas model  | 49        |
| 4.1.3    | Start-up   | 50        |
| 4.1.4    | Steady state   | 54        |
| 4.2      | Verification of the compressor train                               | 58        |



---

|          |   |           |
|----------|---|-----------|
| 4.2.1    | Individual plots . . . . .                        | 58        |
| 4.2.2    | Compressor maps . . . . .                         | 62        |
| 4.2.3    | Site verification . . . . .                       | 64        |
| <b>5</b> | <b>Behaviour analysis</b>                         | <b>67</b> |
| 5.1      | Fuel ramp in STC - a) . . . . .                   | 67        |
| 5.2      | Rotational inertia - b) . . . . .                 | 69        |
| 5.3      | Deactivation of PAC - c) . . . . .                | 72        |
| 5.4      | Gas generator acceleration in NGGL - d) . . . . . | 73        |
| <b>6</b> | <b>Discussion</b>                                 | <b>75</b> |
| 6.1      | Compressor model . . . . .                        | 75        |
| 6.2      | Compressor train . . . . .                        | 75        |
| 6.3      | Verification . . . . .                            | 76        |
| 6.3.1    | Compressor system . . . . .                       | 76        |
| 6.3.2    | Compressor train . . . . .                        | 77        |
| 6.3.3    | Compressor maps . . . . .                         | 77        |
| 6.3.4    | Eischleben and Port Said . . . . .                | 77        |
| 6.3.5    | Behaviour analysis . . . . .                      | 78        |
| <b>7</b> | <b>Conclusions</b>                                | <b>79</b> |
| <b>8</b> | <b>Future work</b>                                | <b>81</b> |
| <b>9</b> | <b>References</b>                                 | <b>83</b> |



# 1. Introduction

For decades Finspång has been a center for industrial manufacturing. The first mill started in the 16th century and flourished with the De Geer family in charge for over 200 years. After a long period of being a major cannon producer for armies in Sweden and Europe the mill had to close in the early 20th century due to competition and the estate was divided into several parts. Two brothers named Birger and Fredrik Ljungström had just founded the company STAL (Svenska Turbinfabrik AB Ljungström) in Stockholm during this time. The brothers saw the potential of Finspångs favorable location and the unused facilities and competence in the area, so they started the production of steam turbines in Finspång. This was the start of the turbine production era in Finspång [1]. In 1953 the first gas turbine order was initiated at STAL and a new business area grew within the company. Many company configurations have followed since then but in 2003 Siemens acquired the company and formed Siemens Industrial Turbomachinery, SIT. In 2013, 100 years since the start of STAL, the company had produced around 2300 steam turbines, 700 gas turbines and consisted of almost 3000 employees [2]. The main business of SIT today is production, development, service and maintenance of gas turbines.

## 1.1 Background

The most common use of an industrial gas turbine is to produce electricity, in a so called power generation (PG) application. Another area of use is to let the gas turbine drive a compressor system and create a compressor train. These compressor trains are used in different applications all over the world. It is common to use compressor trains for transportation of gases, one example of that is transportation of natural gas in pipelines. The gas needs high pressure to be able to travel through the pipeline, and it is desirable to have as long distance between the pump stations as possible. This is why compressor stations with high power output is advantageous. These compressors are in most cases driven by one or several gas turbines, but they can also be driven by an electrical motor. The characteristic preference for both these drivers are that their speed can vary over a large range. This is one of the reasons of why it is important to be able to predict

the systems performance with transient operation, which partly is done in simulation programs [3].

Siemens has during the years developed many transient gas turbine models for calculating performance parameters as temperature, pressure, mass flow and power during transient courses. These are modelled for PG, and not for applications. The MD causes variations of power turbine speed, which changes the system behaviour. A new model for this will make it possible to answer future questions about transient performance in compressor applications and optimize its control system.

During start-up of a compressor driven by a gas turbine there are some phenomena that needs to be avoided. One of this is surge, which occurs when the mass flow is too low and the compressor is unable to produce the required discharge pressure which will emphasize a thermal block in the compressor. The surge phenomena will be explained in detail later in this report. Surge is very harmful for the machine and could cause fatal material damages and large costs. A reliable simulation which gives accurate information about a correct start-up sequence can prevent this and is therefore indispensable.

## **1.2 Objectives**

The purpose of this thesis is to develop a transient model of a driven compressor, based on characteristics. This model will be implemented by connecting it with the model for Siemens Gas Turbine 750 (SGT-750) in order to analyse the behaviour of a complete compressor train during start-up.

### **1.2.1 Problem definition**

The following questions will be analysed and answered in this thesis:

- How well does the developed model correspond to reality?
- How will the gas turbine respond to changes of controller and physical parameters during start-up?

## **1.3 Limitations**

The limitations of the project are listed below:

- The compressor model will mainly be used for simulating the gas turbine behaviour and the compressor models requirement will be put with respect to this.

- The compressor model that will be built is adapted for one specific gas turbine. Despite this, the model will be designed in a way that makes it easy to adapt with a different gas turbine model. This might be advantageous for the future.
- Only necessary changes will be made in the gas turbine model to implement the compressor in this project.
- Only chosen components of the compressor's auxiliary system, which affect the performance of the gas turbine, will be modelled.
- Only components of the control system that affect the running of the compressor or control of the gas turbine will be modelled.

## 1.4 Method

### 1. Literature study

It will be investigated if similar models have been done before, both internal and external. The information shall include both the thermodynamic model of the compressor and auxiliary system, as control systems and valves, for both the compressor system and compressor train.

### 2. Modelling

First a thermodynamic model of a driven compressor will be modelled based on characteristics. Second, the control system and valves will be modelled to enable running of the compressor system and later the complete compressor train, in a correct manner. The modelling will be made in Dymola and use Siemens internal library and Modelica's Media and fluid library. The control system model will be modelled according to specifications from the compressor producer. Existing valve models will be evaluated and adapted to fit the application.

### 3. Implementation

The models that will be designed will be added to the internal version management system, SVN. First step is to design a test model to validate the compressor model without a control system. When the compressor model and control system are designed, the gas turbine will be added for simulation of a complete compressor train.

### 4. Verification

The compressor model will be verified at steady state and the result will be compared with calculations from the compressor producer. Data from a suitable site will be used to verify the compressor train during a chosen transient, tentatively a start-up.

### 5. Behaviour analysis

The verified model will be used to simulate changes of controller parameters and the result will be analysed. The parameters will be chosen based upon how much they affect the gas turbine behaviour.

## 1.5 Tools

- Dymola - Modelling program
- SVN/GITLab - Version management system
- STA-RMS - System for getting measured data from site
- WebPlotDigitizer
- VLE Flash

## 2. Theory

A compressor train consists of many components, not only the compressor. In this chapter the theory of the compressor train and the vital components will be described. The chapter also includes information about tools used in the project.

### 2.1 System description

#### 2.1.1 Mechanical Drive

Mechanical drive (MD) applications of a gas turbine can be found both on and off shore [4]. The largest area of utilization is in pipeline service [5], but they are also widely used in petrochemical industrial complexes. The machines are often aero-derivatives, turbines that were originally designed for aircraft application [4]. These engines have features that suits pipeline applications well; adjustable speed, low operating costs, high reliability and low maintenance costs. Because of these attributes, gas turbines have been used in pipeline applications since the 1950's [5].

All gas turbines follow a specific start-up sequence that is optimized with respect to parameters as rotational speed, surge, torque and fuel flow. Normally a starting engine controls the speed up to approximately 50 %, or before the gas turbine reaches a speed where it can produce the torque to accelerate on its own. The design of the start-up characteristics often differ depending on what application the turbine is used in [6].

#### 2.1.2 Compressor system

A compressor system is used to raise the pressure of a medium. Figure 2.1 shows an example of a compressor system. As [3] writes, a compressor system is often driven by a two shaft gas turbine but a variable speed electric engine can be used for the same purpose. The medium has a low pressure when it enters the compressor, which raises the pressure and temperature of the medium. The cooler is in this case placed directly after the

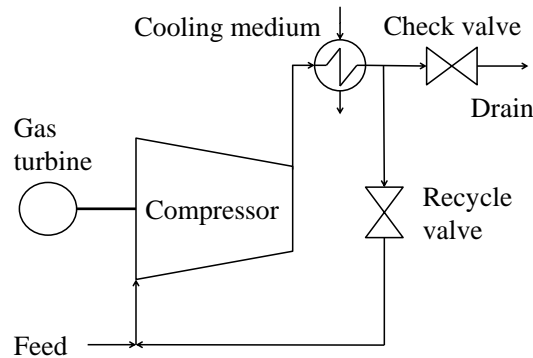


**Figure 2.1: A general compressor system.**

compressor and have the purpose to cool the medium to its inlet temperature. After the cooler a recycle valve is placed which can be opened when needed. This valve controls the anti-surge loop, which has the purpose to avoid surge. Surge is a phenomena that will be described further later in the report. During start-up the anti-surge valve is fully opened and all compressor gas is led to the compressor inlet. In the end of the system, at the drain, a check valve is placed to avoid reverse flow from the downstream pipeline. This can occur during start-up and surge, when the pressure after the compressor is below the system back pressure.

## 2.2 Compressor

There are four main types of compressors; rotary, reciprocating, centrifugal and axial compressors. The rotary compressor occurs in different types, but the most common consists of two screw-formed parallel axes, rotating against each other. The screws forces the medium through, reduces the area and thereby increase the pressure of the medium [7]. The reciprocating compressor works in a similar way and have a basic design not so different from the piston engine, see Figure 2.2. The medium flows through an inlet valve, compresses with the energy from the piston and exits with a higher pressure [8]. The axial compressor has, unlike the reciprocating compressor, axial flow through the whole process. The compressor consists of several stages of stators and rapidly rotating impellers. The impellers increase the velocity of the medium and the stators transform the velocity into pressure rise [4]. The centrifugal compressor is the compressor used in this project. This type consists of a rotating and a diffusing part that is perpendicular to the flow inlet [4] and will be described in detail in section 2.3 Centrifugal compressor.



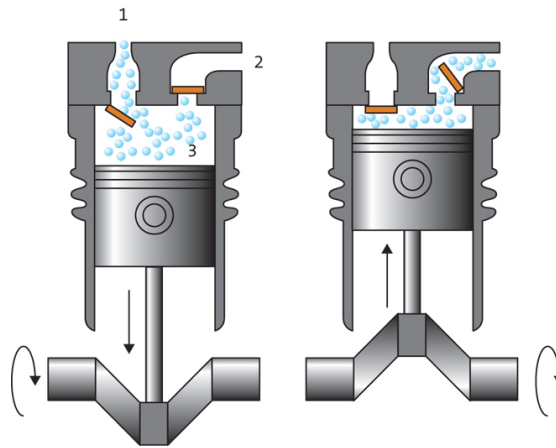


**Figure 2.2: Basic function of reciprocating compressor (Figure: [8])**

### 2.3 Centrifugal compressor

The centrifugal compressor is a continuous flow compressor and consists of inlet guide vanes, an inducer, a rotating impeller, a number of stationary diverging passes called the diffuser and a volute. Figure 2.3 shows a sketch of a typical centrifugal compressor. The size of a centrifugal compressor varies in the range of pressure ratio 3:1 per stage to as high as 12:1 which has been achieved in experimental models. In petrochemical industry however, the pressure ratio is normally below 3.5:1 [4].

The main parts of the compressor are the impeller and the diffuser, which are the components where the pressure rise is achieved. The incoming gas enters the compressor through an intake duct and if Inlet Guide Vanes (IGV) are used, the gas is pre-whirled before being sucked into the inducer. The gas often enters the impeller axially with respect to the drive shaft and its speed and pressure is increased by the rotating impeller. When going through the vanes of the impeller the flow direction changes from axial to radial and the static pressure of the gas is increased from the eye to the tip of the impeller. The gas then flows into the diffuser, where the velocity is decreased approximately to the same velocity of the gas at the inducer. This will further increase the static pressure of the gas. According to [9], a centrifugal compressor is often designed so that half of the pressure rise occurs in the impeller and half in the diffuser. After the diffuser the gas leaves the compressor stage through the volute and discharges with a significantly higher pressure.

### 2.4 Energy and mass balance

When calculating thermodynamic relations for a compressor, a control volume can be put as in Figure 2.4. According to [11] the change in total energy in the system can

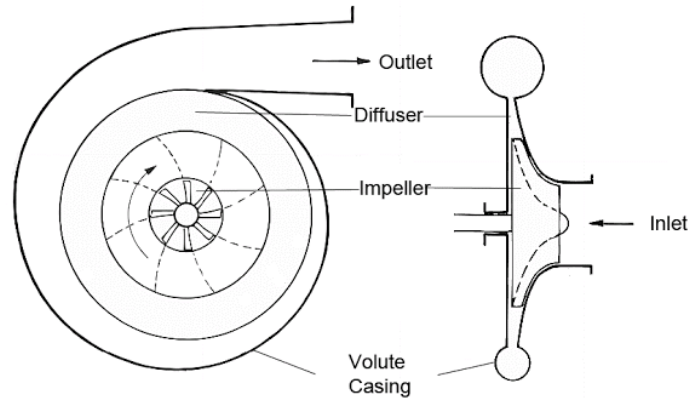


**Figure 2.3: Centrifugal compressor illustration. (Figure: [10])**

be expressed with equation (2.1), where  $KE$  represents the kinetic energy and  $PE$  the potential energy. Equation (2.2) shows an explanatory version of the equation.

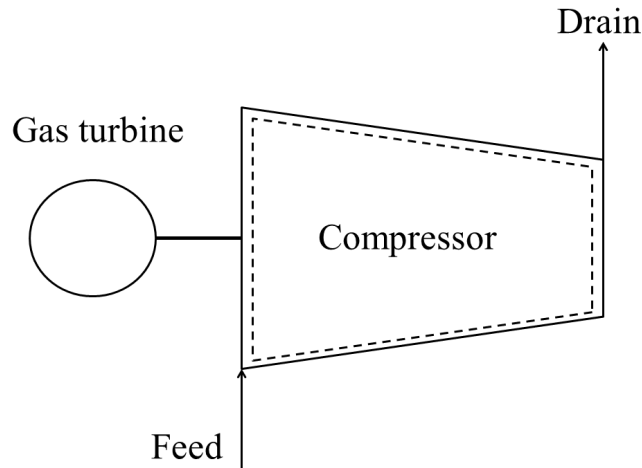


**Figure 2.4: Control volume over compressor.**

$$E_{in} - E_{out} = \Delta E_{system} \quad (2.1)$$

$$[U + KE + PE]_{in} - [U + KE + PE]_{out} = [U + KE + PE]_{system} \quad (2.2)$$

Since it is a stationary system the changes in potential and kinetic energy are zero, the same applies to the mass flow ( $\Delta KE = \Delta PE = \Delta \dot{m} = 0$ ). This gives  $U_{in} - U_{out} = \Delta E_{system}$ . The control volume does not absorb any potential energy, which means that the initial and final states are identical,  $\Delta E_{system} = E_2 - E_1 = 0$ .

Energy can be transferred to and from a system in three ways; heat ( $Q$ ), work ( $W$ ) and mass ( $m$ ). The mass balance is defined in equation (2.3), and transforms equation (2.2) into equation (2.4).

$$\dot{m}_{in} - \dot{m}_{out} = \Delta\dot{m}_{system} \quad (2.3)$$

$$[Q + W + E_{mass}]_{in} - [Q + W + E_{mass}]_{out} = \Delta E_{system} = 0 \quad (2.4)$$

In the analyse of a compressor it is assumed that  $Q_{in} = Q_{out} = W_{out} = 0$ . This gives equation (2.5) where  $h$  denotes the enthalpy,  $h = u + pv$ , [11].

$$\begin{aligned} W_{in} + E_{mass, in} + E_{mass, out} &= 0 \\ \Rightarrow W_{in} + [mh]_{in} + [mh]_{out} &= 0 \\ \Rightarrow W_{in} + \dot{m}(\Delta h) &= 0 \end{aligned} \quad (2.5)$$

## 2.5 Ideal gas model

As [12] writes, the ideal gas model is given by

$$pv = ZRT \quad (2.6)$$

where  $R$  is defined as

$$R = \frac{\bar{R}}{M} \quad (2.7)$$

where  $\bar{R} = 8.314$ . The compressibility factor for the gas,  $Z$ , does affect the accuracy of the ideal gas model and is defined as

$$Z = \frac{vP_R}{RT_R} \quad (2.8)$$

where the reduced pressure  $p_R = p/p_c$  and reduced temperature  $T_R = T/T_c$ .  $p_c$  and  $T_c$  represent the critical pressure and temperature. The relation between  $Z$ ,  $p_R$  and  $T_R$  can be seen in Figure 2.5. When  $p_R$ , is small and  $T_R$  is large the value of  $Z$  is close to 1. If so, equation (2.6) can be rewritten to equation (2.9) [12].

$$pv = RT \quad (2.9)$$

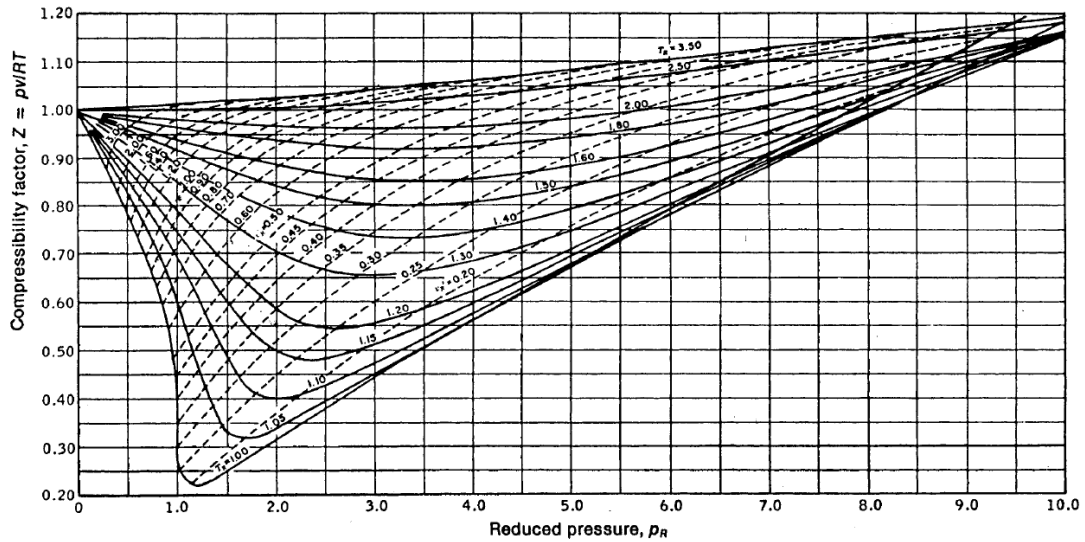


Figure 2.5: Compressibility factor  $Z$ . (Figure: [12])

## 2.6 The momentum equation and the Euler work equation

A much useful principle in mechanics is Newton's second law of motion, the momentum equation. The equation relates the total forces acting on a fluid element to its acceleration. Applying the equation in turbomachinery it describes the forces acting on turbine or compressor blades caused by deflection or acceleration of fluid passing the blades. In a system that consists of mass  $m$ , the sum of all forces acting on  $m$  along a given direction is equal to the change of total momentum of the system in time, along the given direction:

$$\Sigma F_x = \frac{d}{dt}(mc_x) \quad (2.10)$$

where  $F_x$  and  $c_x$  is the force and velocity in the given direction. For a one-dimensional steady flow process the momentum equation becomes:

$$\Sigma F_x = \dot{m}(c_{x2} - c_{x1}) \quad (2.11)$$

The second law can form equation (2.12) which describes the torque of all external forces acting on an axis  $A - A$  fixed in space.  $r$  denotes the distance to the mass center from the axis of rotation measured along the normal to the axis and  $c_\theta$  the perpendicular velocity to both the radius and the axis.

$$\tau_A = m \frac{d}{dt}(rc_\theta) \quad (2.12)$$

## 2. THEORY

---

This form of Newton's second law is important in analyzing the amount of energy being transferred in a turbomachine process. Equation (2.12) can be written as equation (2.13) for a one-dimensional steady flow process with notations shown in Figure 2.6.

$$\tau_A = \dot{m}(r_2 c_{\theta 2} - r_1 c_{\theta 1}) \quad (2.13)$$

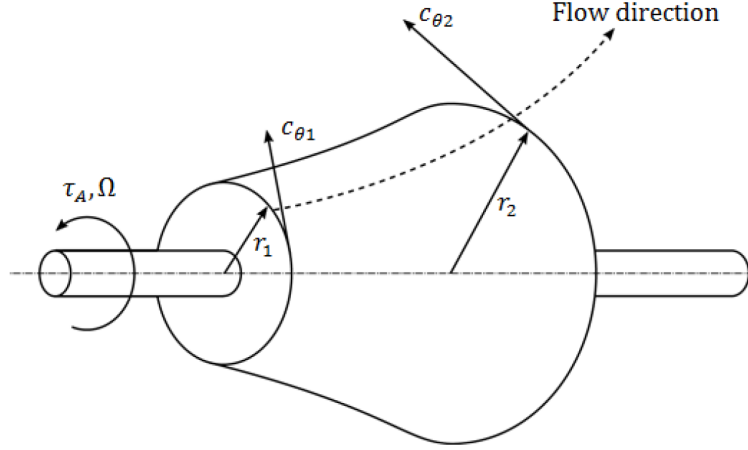


**Figure 2.6: Control volume for a turbomachine (Figure: [13])**

The Euler compressor equation can be derived using equation (2.13), the blade speed,  $U = \Omega r$ , where  $\Omega$  is the angular velocity.

$$\dot{W}_c = \tau_A \Omega = \dot{m}(U_2 c_{\theta 2} - U_1 c_{\theta 1}) \quad (2.14)$$

The equation describes the rate at which the rotor does work on the fluid. The specific work done in a pump or compressor is derived as

$$\Delta W_c = \frac{\dot{W}_c}{\dot{m}} = (U_2 c_{\theta 2} - U_1 c_{\theta 1}) > 0. \quad (2.15)$$

Equation (2.15) is called the *Euler's pump equation* and for a turbine, where the fluid does work on the rotor the equation is reversed.

$$\Delta W_t = \frac{\dot{W}_t}{\dot{m}} = (U_1 c_{\theta 1} - U_2 c_{\theta 2}) > 0. \quad (2.16)$$

Thus, the equation above is called the *Euler's turbine equation* [13].

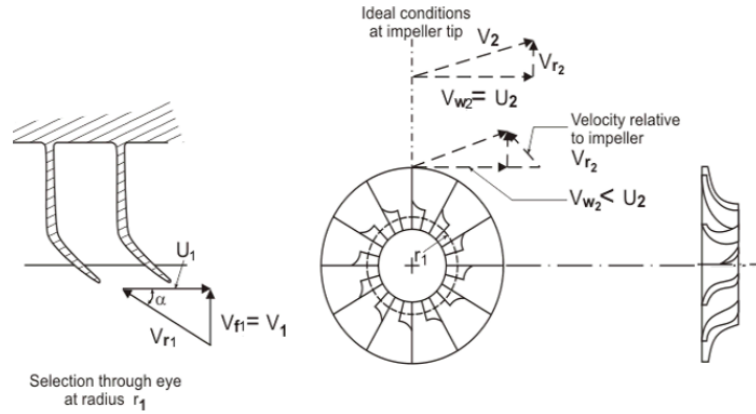


**Figure 2.7: Centrifugal compressor nomenclature. (Figure: [9])**

## 2.7 Work done

The work done in the compressor is solely in the impeller and therefore all the energy absorbed by the gas can be determined by the inlet and outlet conditions of the impeller. The Euler pump equation (2.15) describes the theoretical amount of work imparted by the gas as it goes through the impeller, and with the notation in Figure 2.7 the equation is modified into equation (2.17).

$$\Delta W_c = \frac{\dot{W}_c}{\dot{m}} = \tau \Omega = U_2 V_{w2} - U_1 V_{w1} \quad (2.17)$$

With an axial inlet ( $V_{w1} = 0$ ) the equation transforms into equation (2.18).

$$\Delta W_c = U_2 V_{w2} \quad (2.18)$$

The work done on the gas can also be described by the slip factor,  $\sigma$ , according to equation (2.19).

$$\Delta W_c = \sigma U_2^2 \quad (2.19)$$

Slip occurs when the gas that is trapped between the vanes is being reluctant to move with the impeller due to its inertia. This resulting in a difference between the impeller speed,  $U_2$ , and the tangential component  $V_{w2}$ , i.e a deviation from the ideal conditions. How large this deviation is depends on the number of impeller vanes, a greater number of vanes means a smaller slip. Though, a greater number of vanes lead to a decrease in flow area and thereby an increase in friction, due to an increase in velocity for a constant mass flow. The slip factor is defined as  $V_{w2}/U$  and for radial vanes impellers  $\sigma$  can be approximated with equation (2.20).

$$\sigma = 1 - \frac{0.63\pi}{n} \quad (2.20)$$

where  $n$  is the number of vanes. Introducing the power input factor,  $\psi$ , which represents friction and other losses the work done can be written as equation (2.21).

$$\Delta W_c = \psi \sigma U_2^2 \quad (2.21)$$

With no energy being added in the diffuser and with the isentropic efficiency taken into account, the amount of work used in the compressor to raise the stagnation pressure ratio can be written as equation (2.22) where  $\gamma$  is the ratio between the specific heats  $c_p$  and  $c_v$ .

$$\frac{p_{03}}{p_{01}} = \left( \frac{T'_{03}}{T_{01}} \right)^{\frac{\gamma}{\gamma-1}} = \left[ 1 + \frac{\eta_{is}(T_{03} - T_{01})}{T_{01}} \right]^{\frac{\gamma}{\gamma-1}} = \left[ 1 + \frac{\eta_{is}\psi\sigma U^2}{c_p T_{01}} \right]^{\frac{\gamma}{\gamma-1}}. \quad (2.22)$$

The stagnation temperatures in and out of the diffuser is unchanged,  $T_{03}=T_{02}$ , thus,  $T_{03} - T_{01} = T_{02} - T_{01}$  and the isentropic efficiency is assumed according to equation (2.23). The indices 01 and 02 indicates the inlet and outlet of a compressor respectively in equation (2.23) [9].

$$\eta_{is} = \frac{T'_{02} - T_{01}}{T_{02} - T_{01}} = \frac{\left( \frac{p_{02}}{p_{01}} \right)^{\frac{\gamma-1}{\gamma}} - 1}{\left( \frac{T_{02}}{T_{01}} \right) - 1} \quad (2.23)$$

Equation (2.23) also shows the connection between temperature and pressure during a compression or expansion process and the T-S diagram for a typical compression process is shown in Figure 2.8. The dotted line represent an isentropic compression and the filled a real compression.

## 2.8 Compressor characteristics

The performance of a centrifugal compressor can be described in many ways, one way is to plot the outlet pressure and temperature against mass flow for various fixed rotational speeds of the rotor. To describe the compressor in such a way is however not the most common way to do it because of the dependence of other variables such as inlet conditions and gas properties of the working medium. Therefore the technique of dimensional analysis is often used where the variables are formed into smaller dimensionless groups, which enables the performance of various machines to be compared to each other. The

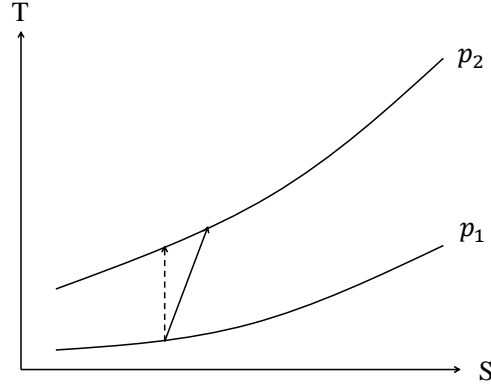


**Figure 2.8: Temperature-entropy diagram for a pressure rise.**

characteristics of a compressor can then be specified by the curves shown in Figure 2.9. The dimension analysis, which is further described in [9], results in four common dimensionless groups, with definitions according to nomenclature:

$$\frac{p_{02}}{p_{01}}, \frac{T_{02}}{T_{01}}, \frac{\dot{m}\sqrt{RT_{01}}}{D^2 p_{01}}, \frac{ND}{\sqrt{RT_{01}}}$$

Accordingly, the performance of a machine regarding variations in outlet pressure and temperature with mass flow, rotational speed and inlet conditions can be expressed as a function of the dimensionless groups. When a machine of fixed size is viewed and a certain gas is compressed, the variables gas constant,  $R$  and the diameter,  $D$ , can be overlooked which results in equation (2.24).

$$f\left(\frac{p_{02}}{p_{01}}, \frac{T_{02}}{T_{01}}, \frac{\dot{m}\sqrt{T_{01}}}{p_{01}}, \frac{N}{\sqrt{T_{01}}}\right) = 0 \quad (2.24)$$

The two groups  $\dot{m}\sqrt{T_{01}}/p_{01}$  and  $N/\sqrt{T_{01}}$  are usually called the non-dimensional mass flow and rotational speed and are represented in a typical plot as the x-axis and the various fixed parameter, respectively, which can be seen in Figure 2.9. This is a common way to express the compressor characteristics, though, any combination of two dimensionless groups can be plotted against each other, for a third group with various fixed values. Instead of the non-dimensional mass flow and rotational speed the equivalent flow,  $\dot{m}\sqrt{\theta}/\delta$  and equivalent speed,  $N/\sqrt{\theta}$  can be used, where  $\theta = T_{01}/T_{ref}$  and  $\delta = p_{01}/p_{ref}$ . The reference values are usually atmospheric pressure and 288 K. The non-dimensional mass flow and rotational speed can also be interpreted as based on Mach-numbers and written as equation (2.25) and (2.26) respectively.



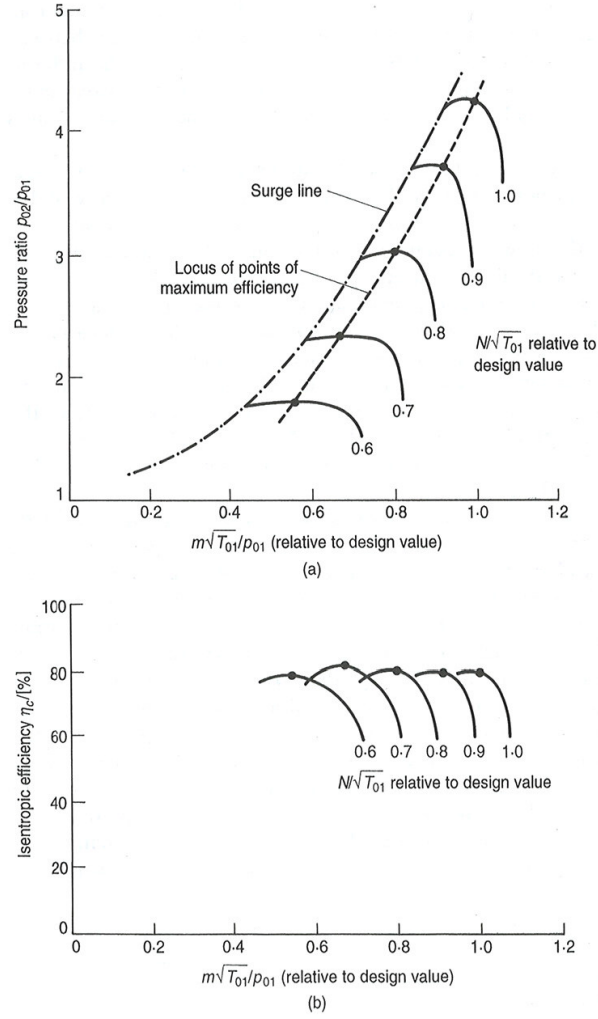


**Figure 2.9: Compressor map. Figure (a) shows the non-dimensional mass flow against the pressure ratio for different rotational speeds. Figure (b) shows the non-dimensional mass flow against the isentropic efficiency for different rotational speeds. (Figure: [9])**

$$\frac{\dot{m}\sqrt{RT}}{D^2p} = \frac{\rho AC\sqrt{RT}}{D^2p} = \frac{pAC\sqrt{RT}}{RTD^2p} \propto \frac{C}{\sqrt{RT}} \propto M_F \quad (2.25)$$

$$\frac{ND}{\sqrt{RT}} = \frac{U}{\sqrt{RT}} \propto M_R \quad (2.26)$$

The equations above shows that the parameters can be regarded as a flow Mach number,  $M_F$ , and rotational speed Mach number,  $M_R$ .

If the stagnation temperature ratio is plotted in the same way as the stagnation pressure ratio it is possible to construct Figure 2.9b where the efficiency is plotted against the

non-dimensional mass flow and rotational speed. The isentropic efficiency can be expressed as equation (2.23).

Another way to express the compressor performance characteristics is shown in Figure 2.10 where the dotted lines are so called efficiency islands. In both figures the parameter on the y-axis is the pressure ratio with the surge line plotted as a restricting line to the left in the figure. Surge is a phenomenon that makes the operation of the compressor unstable and is further described in section 2.9 Rotating stall and surge. It can be seen that the constant speed lines in Figure 2.10 becomes vertical and is bunched together when the speed is increasing, which is a consequence of choking of the compressor. Thus the compressor is constrained by the surge phenomenon to the left and the choking condition to the right. The behaviour of the speed lines can be explained with Figure 2.11 where a single speed line is plotted against mass flow and pressure ratio. As the valve opens and more flow is allowed into the compressor, the pressure ratio and the efficiency reaches a maximum value, point B. The increase in flow means that the diffuser starts contributing to the pressure ratio which increases, and according to equation (2.23) the isentropic efficiency increases. A further increase in mass flow to point E will result in a drop in pressure ratio caused by the air angles being different to the vane angles, which causes the flow to breakaway, thus a decrease in efficiency and pressure ratio due to friction. If the mass flow is increased beyond point E, it will lead to the phenomena called "choking" where the mass flow cannot be increased further, due to the Mach number being over one at the minimum area of the compressor [4]. This is caused by a decrease in density, which means that the radial velocity must increase. At constant rotational speed that lead to an increase in absolute velocity, hence an increase in angle of incidence at the diffuser vane, which finally leads to "choking" of the compressor [9].

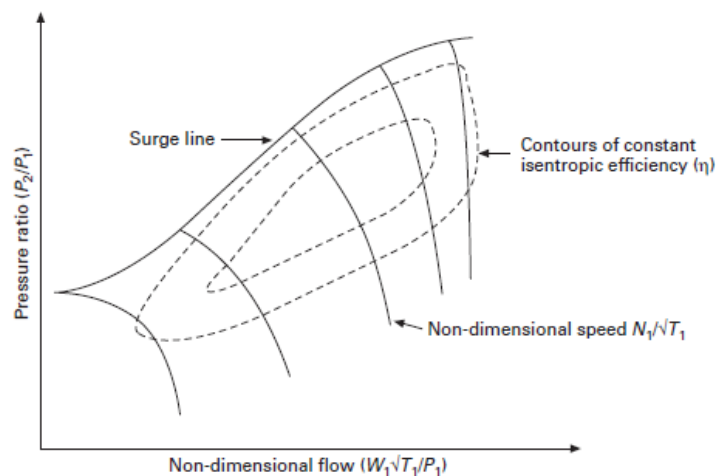


**Figure 2.10: Compressor map. (Figure: [14])**

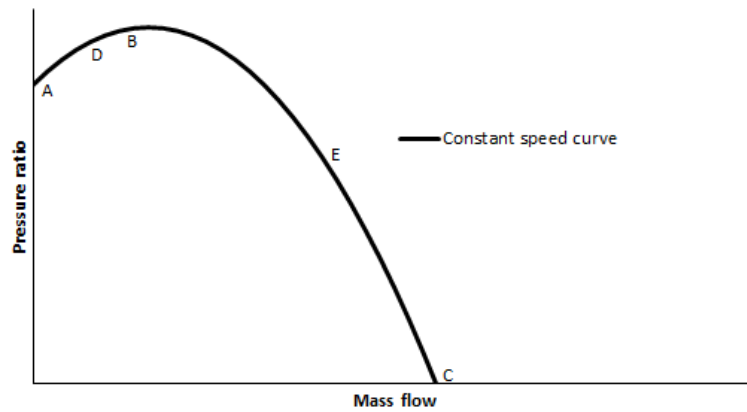


Figure 2.11: Plot of one speed line.

## 2.9 Rotating stall and surge

When the compressor is driven at a fixed speed, the flow is steady and there are small deviations in pressure and velocity. There are nevertheless circumstances that will make the flow profile very unstable and unpredictable. Two phenomena that will cause this are called *rotating stall* and *surge* [15]. Let us start with describing how rotating stall is initiated.

As [14] writes, reduced mass flow gives an increased rotor inlet air angle. This can cause flow separating as it passes over blades, see Figure 2.12. Part of the flow that was meant for channel C, goes through channel B instead and forces channel B to stall. This pattern moves along the impeller and rotates, relative to the rotor, in opposite direction with approximately half the speed of the rotor, initiating rotating stall [14]. The phenomena causes large vibratory stresses in the blading of the compressor and can lead to high blade stress levels [15]. Rotating stall decreases the efficiency of the stage, but the compressor can in some cases still be able to perform. A danger with rotating stall is that it can lead to surge, which has negative effect on both the performance and the mechanical parts of the compressor [14].

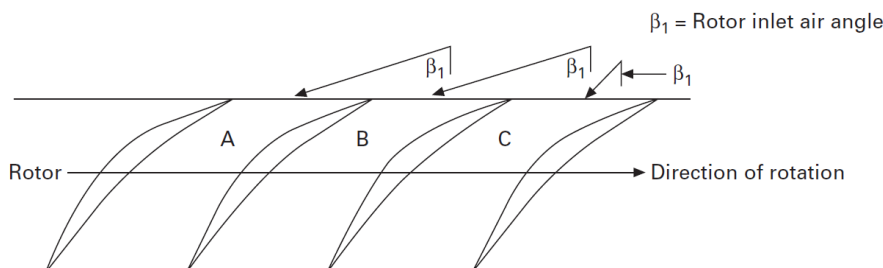


Figure 2.12: This figure shows how air is pushed over channels, and can introduce rotating stall. (Figure: [14])

Suppose the mass flow by any reason is reduced and rotating stall is initialized. The stall develops circularly and finally covers the whole flow annulus. This causes a significant reduction in efficiency and the compressor is no longer able to perform the required pressure rise. Because of the higher back pressure of the compressor the flow will be reversed and start to go backwards. The reversed flow will lower the downstream pressure and at some point the flow will return to its normal flow direction. Nevertheless, if the conditions that first initialized surge remains, the surge can re-occur. This change of flow direction can occur with a high frequency and be very destructive for the compressor [14]. The high pressure gradients contributes to high temperature gradients which has an adverse effect on the blade life expectancy [16].

## 2.10 Polytropic efficiency using the sT-method

In simple calculations the efficiency is calculated for the turbine or compressor as a whole. In fact this may lead to misleading calculation results when performing cycle calculations. As can be seen in Figure 2.8 the isobars diverge as entropy increases. This results in that the vertical distance between pressure lines (= temperature rise in each interval) differ throughout the process. As the efficiency depends on temperature rise the difference will increase with the number of stages in the compressor. To handle this differently another efficiency is used, the *polytropic* efficiency. The polytropic efficiency is defined as the isentropic efficiency of an infinitesimal small stage in the process, which is a more accurate definition than the isentropic efficiency of the whole compressor [9].

As [17] writes, the polytropic efficiency is normally calculated with equation (2.27). No derivation of this equation will be given here, hence it can be further studied in [17].

$$1 - \left(\frac{p_2}{p_1}\right)^{\frac{\gamma-1}{\eta_{pol}\gamma}} = \frac{1 - \left(\frac{p_2}{p_1}\right)^{\frac{\gamma-1}{\gamma}}}{\eta_{is}} \quad (2.27)$$

Equation (2.27) assumes that the gas is an ideal gas with constant  $c_p$ . In performance programs that are used in this project the gas is handled as an semi ideal gas with a  $c_p$  that depends on temperature but not pressure. Due to this issue it would be advantageous to calculate the polytropic efficiency in a more accurate way. The sT-method is presented by [17] and is the one used in this project. In this method the entropy is used, and not the pressure as above. The efficiency is calculated with equation (2.28), with definitions according to Figure 2.13.  $s_T$  is the entropy for the outlet temperature at inlet pressure.

$$\eta_{pol} = \frac{s_T - s_2}{s_T - s_1} \quad (2.28)$$

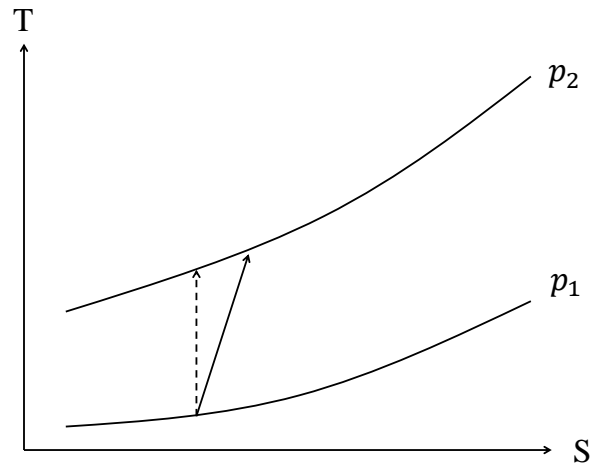


**Figure 2.13: Definition of parameters for the sT-method.**

## 2.11 Gas turbine

The gas turbine is a powerful and efficient power source. It transforms the energy in liquid or gaseous fuels into mechanical work. Historically the aerospace engines have been the leaders in this technology, due to the hard demands on the engines. They have to be durable for high performance, high reliability and last for many start-up sequences. In the 1990s the aero-derivative gas turbines were introduced, which improved the performance of industrial gas turbines. In early 1950s the efficiency was around 15 %, but today it can be as high as 45-50 %. Industrial gas turbines were between 1960s and 1980s mainly used for peak-load, but as technology developed it became a great competitor against other power sources, even at base-load [4].

Figure 2.14 shows the working principle of a single-shafted gas turbine. The medium is first flowing through the compressor where the energy from the shaft increase the pressure of the medium. The medium is then heated in the burner, where fuel is injected to increase the temperature. In the turbine the pressure and temperature energy is transformed into rotational energy. Some of the energy is absorbed by the compressor and the excess energy is used by the load through a mechanical shaft. The four thermodynamic stages in the process are defined in the ideal Brayton cycle which can be seen in Figure 2.15. The numbers 1-4 represent the different components of the gas turbine. The two (ideal) isobaric processes represent the combustor and cooler, the isentropic represent the compressor and turbine. In the general model there is no cooler for the outlet flow, instead this is represented by the ambient environment [4].

If a single-shaft gas turbine is used for MD there is often a need to unload the driven component during start-up to reduce the torque needed [6]. A multi-shaft turbine has the advantage that the gas generator and power turbine are not connected with a shaft and thereby are able to rotate with different speeds. This makes it easier to start the turbine

with the driven load connected [18].

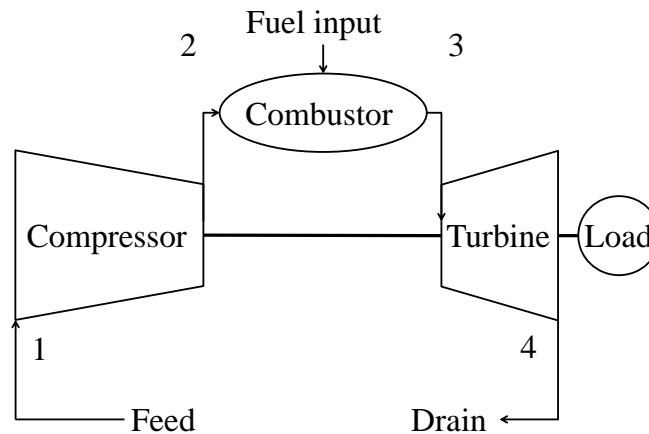


**Figure 2.14: Gas turbine working principle.**

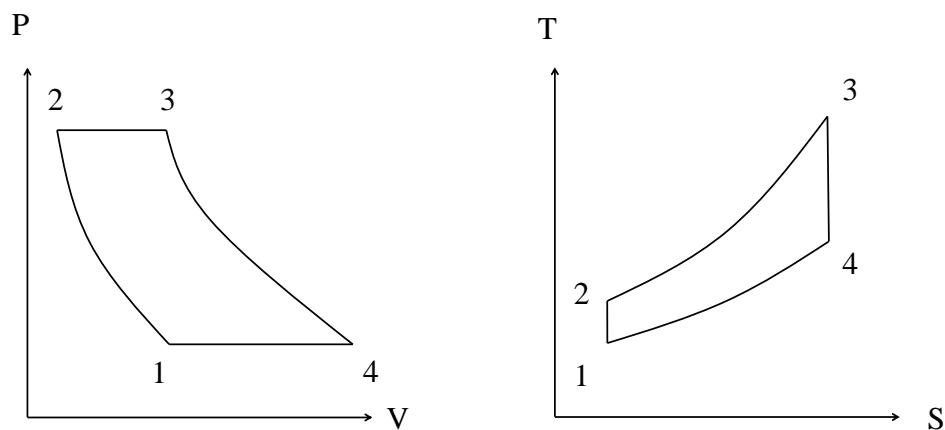


**Figure 2.15: The Brayton cycle.**

As seen in Figure 2.14 this gas turbine only have one shaft. Though, gas turbines can be divided into two different groups, single-shafted and multi-shafted gas turbines. The working principle of a multi-shafted gas turbine is similar to a single-shafted, with the natural difference that there is more than one shaft, see Figure 2.16. The single-shaft gas turbine is often used in purpose of PG, while the multi-shaft could be used for both PG and in MD applications. In a multi-shaft gas turbine one shaft is connected to the compressor and one to the load which allows the two shafts to rotate at different speeds. The multi-shaft cycle has advantages when it comes to part load and load variations due to its high torque at low rotational speeds, which is why they often appear in MD applications [4].

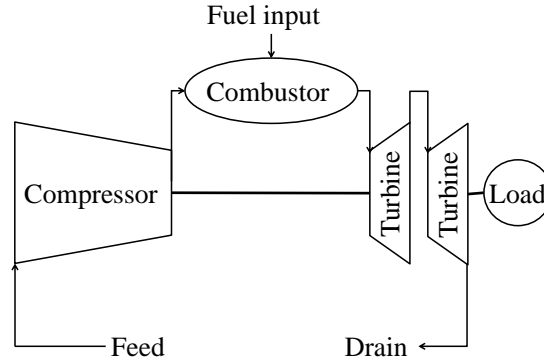


Figure 2.16: Gas turbine working principle, two-shafted.

## 2.12 Heat transfer

The concept of heat transfer is described in [19] as energy being transferred from the hot to the cold part of a substance, or from a body with a higher temperature to a body with a lower temperature. The bodies do not have to be in touch with each other, though a temperature difference has to exist for the heat transfer to take place. Heat can be transferred in three ways: conduction, convection and radiation. The principle of heat transfer in a cooler, or heat-exchanger, is shown in Figure 2.17.

The heat transfer in a cooler can be written as equation (2.29)

$$\dot{Q} = HTC \cdot A \cdot \Delta T_m \quad (2.29)$$

where  $HTC$  is the overall heat transfer coefficient,  $A$  the area over which heat transfer occurs and  $T_m$  the mean temperature difference. Two ways to analyse a heat exchanger is the LMTD-method and the  $\epsilon$ -NTU method which are further described in [19]. Equation (2.30) states the first law of thermodynamics for a closed system.

$$\dot{Q} = W_k + \frac{dU}{dt} \quad (2.30)$$

where  $\dot{Q}$  is the heat transfer rate,  $W_k$  is the work transfer rate and the derivative  $dU/dt$  is the rate of change of internal energy. In a cooler where no work is done except  $pdV$  the transforms into equation (2.31).

$$\dot{Q} = p \frac{dV}{dt} + \frac{dU}{dt}. \quad (2.31)$$

Equation (2.31) has two cases, one for a constant volume process, equation (2.32),

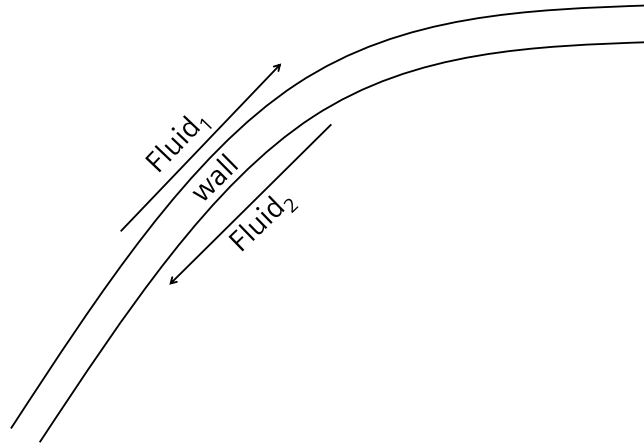


**Figure 2.17: Heat transfer in a cooler. (Figure: [19])**

$$\dot{Q} = \frac{dU}{dt} = \dot{m}c_v \frac{dT}{dt} \quad (2.32)$$

and one for a constant pressure process, equation (2.33),

$$\dot{Q} = \frac{dH}{dt} = \dot{m} \cdot c_p \frac{dT}{dt} \quad (2.33)$$

where  $H$  is the enthalpy ( $H = U + pV$ ). To describe heat transfer with the First law of thermodynamics it has to be combined with the transport laws. The Fourier's law, Newton's law of cooling and the Stefan-Boltzmann's law handles the three ways heat can be transferred and are further described in [20].

## 2.13 System control

Controlling of driven compressors are indispensable for several reasons. One reason is that controllers have great influence on the economy of the compressor, in respect of energy requirements, downtimes, life expectancies and product quality. Another reason is to protect supporting system components or to prevent the compressor from going into surge during start-up and normal operation conditions.



### 2.13.1 Anti-surge control

As mentioned above, surge is an undesirable phenomena, why recycle valves often are used. The recycle valve redirects some of the flow at the outlet of the compressor to the inlet in order to keep the flow through the compressor above the surge limit. Because of rapid changes in system parameters safety measures are required and a control line is often used. The control line is normally stipulated at a distance of 5-10 % to the right of the surge line, i.e at 5-10% higher than the surge mass flow for a constant rotational speed. When the control line is reached, the recycle valve (see Figure 2.1) opens and the operating point is moved away from surge. The surge margin can be calculated as (2.34)

$$SM = \frac{\dot{m}_{op} - \dot{m}_s}{\dot{m}_s} \quad (2.34)$$

where  $\dot{m}_{op}$  and  $\dot{m}_s$  is the mass flow at the operating point and the mass flow on the surge line respectively. For calculating with volume flow,  $\dot{m}$  is simply replaced with  $\dot{V}$ . The disadvantage of having a recycle line is the fact that the natural gas has to go through the compressor several times, which increase the energy consumed by the compressor, thus, decreases the efficiency. Though the recycle valve can be seen as economical compared to the damages that could arise [21].

### 2.13.2 PID-controller

A very common controller in the process industry is the PID-controller. The PID-controller works as a control loop feedback mechanism and has the ability to eliminate offsets through integral action and to predict the future through derivative action. The principle of a feedback controller is shown in Figure 2.18. The feedback of this type is normally called negative feedback where  $y$  represents the operating value,  $y_{sp}$  the set-point value,  $e = y_{sp} - y$  the control error and  $u$  the control variable in the figure. When an error is present in the controller loop, it has to be eliminated in the best manner. One way in achieving this is the use of a PID-controller. The PID-algorithm can be described as equation (2.35),

$$u(t) = K \left( e(t) + \frac{1}{T_i} \int_a^b e(\tau) d\tau + T_d \frac{de(t)}{dt} \right) \quad (2.35)$$

where the three terms represents the P-term, the I-term and the D-term respectively. The P-term is proportional to the error, the I-term is proportion to the integral of the error and the D-term proportional to the derivative of the error.  $K$  is the proportional gain,  $T_i$  the integral time,  $T_d$  the derivative time,  $t$  is the time and  $\tau$  is the variable of integration. The PID-algorithm can also be represented by the transfer function (2.36).

$$G(s) = K \left( 1 + \frac{1}{sT_i} + sT_d \right) \quad (2.36)$$

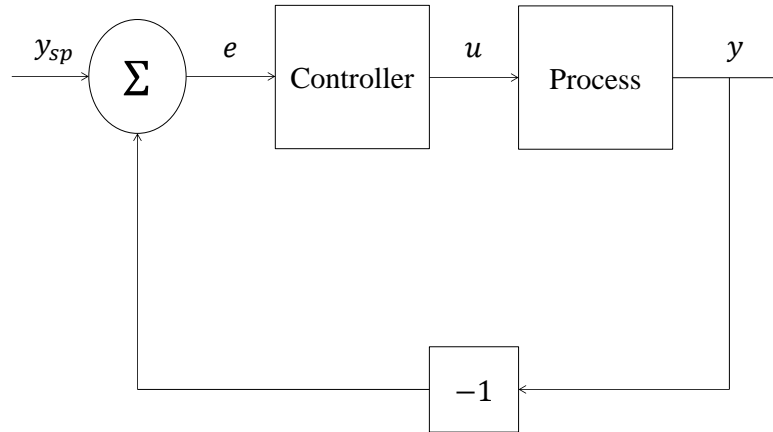


**Figure 2.18: Block diagram of a simple feedback mechanism.**

The simplest form of the PID-controller is the P-only controller which reduces equation (2.35) to equation (2.37).

$$u(t) = Ke(t) + u_b. \quad (2.37)$$

The control action of the P-only controller is proportional to the error. When the control error is zero the control variable,  $u(t)$ , becomes equal to  $u_b$  (the bias or reset), which is chosen in a way so that the control error is zero at a given set-point or as a fixed value of  $(u_{max} - u_{min})/2$ . A high value of  $K$  gives a faster control and a smaller control error, but with the possibility of instability in the system which is illustrated in Figure 2.19.

If it is necessary to eliminate the error completely, the addition of the integral term is needed, which gives us the PI-controller. The integral term assures that the process output agrees with the set-point due to the integration of the error over time. The PI-controller is described by equation (2.38)

$$u(t) = K(e(t) + \frac{1}{T_i} \int_a^b e(\tau) d\tau). \quad (2.38)$$

For large values of  $T_i$  the response of the system is slower in approaching the set-point, but with less oscillations and instability which can be seen in Figure 2.20.

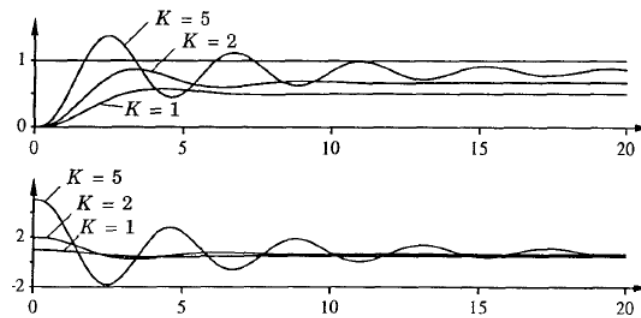


**Figure 2.19:** The upper diagram shows the set-point,  $y_{sp} = 1$ , and the process output,  $y$ . The lower diagram shows the control signal  $u$  for different gain values,  $K$ . (Figure: [22])

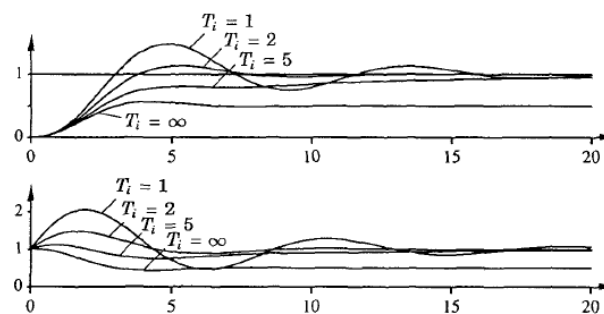


**Figure 2.20:** The upper diagram shows the set-point,  $y_{sp} = 1$ , and the process output,  $y$ . The lower diagram shows the control signal  $u$  for different integral times,  $T_i$ , with  $K = 1$ . (Figure: [22])

The derivative part can be added to improve the stability of the closed loop, which makes the PID-controller complete and forms equation (2.35). With the use of the derivative of the error the controller predicts the behaviour of the error and will be able to respond more quickly than a controller without derivative action. Different values of the derivative time,  $T_d$  is shown in Figure 2.21, where the larger  $T_d$  value dampens the oscillations at first but further increasing of  $T_d$  decreases the damping. For most processes the PID-controller is sufficient and a more complex controller is not needed. A problem that follows with the PID-controller is the tuning of the parameters. This can be done in several ways, for example with the Ziegler-Nichols methods [22].

## 2.14 Start-up sequence

As stated by [4], the start-up sequence is one of the major functions of a control system. Normally the start-up sequence is in charge of the operation up to 50 % of the maximum rotating speed. In the compressor train simulated in this project there is one controller

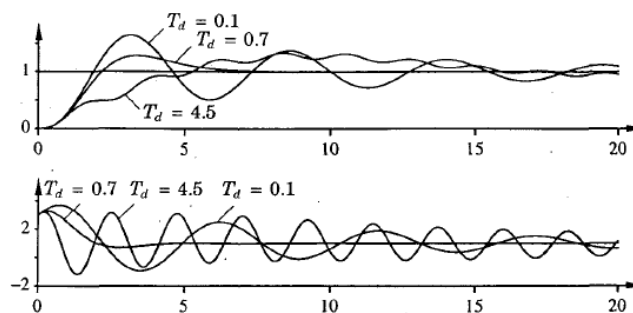


**Figure 2.21:** The upper diagram shows the set-point,  $y_{sp} = 1$ , and the process output,  $y$ . The lower diagram shows the control signal  $u$  for different derivative times,  $T_d$ , with  $K = 3$  and  $T_i = 2$ . (Figure: [22])

for the compressor and one for the gas turbine, and they have different tasks during start-up. How the start sequence is designed depends on many factors such as compressor manufacturer, model and if it is driven by a gas turbine or electrical engine [4].

If a compressor system is equipped with an anti-surge loop the valve is normally fully open during start-up, as mentioned. The mechanisms that control the inlet flow, as guide vanes or inlet throttles, are in their minimum position to keep a low inlet flow. This is due to the low torque at low rotational speeds. The anti-surge loop strives to have a high mass flow through the compressor. When the start-up procedure is finished the anti-surge valve closes and another control system takes over the operation of the system [21].

The gas turbine has in turn its own start-up sequence, designed according to firing temperature, torque at low speeds and many other parameters [4]. How the sequence is designed depends on the configuration, if it is a single- or multi-shafted turbine and if it is a PG or MD application. An electrical starter engine is used from stationary to a certain speed level, and the power of this engine may vary a lot. Power requirements for a 150 MW gas turbine can be as high as 5 MW, and for a gas turbine of 30 MW with a free power turbine the requirements can be as small as 20 kW. The power requirements for a gas turbine with free power turbine is always less than for a single-shafted, because the gas generator being the only part being accelerated and not the whole rotor [9]. The control system that controls the start-up sequence will be further described in chapter 3.3 [Dymola model of gas turbine control system](#).

## 2.15 Purge

In the gas turbine there are explosive fluids, as the fuel, which can cause fatal damages if burning or exploding at the wrong time and wrong place. Before start these fuels can exist in shape of liquid or vapour in places where it is not supposed to be. To solve this problem the gas turbine is purged with ambient air before start. The purge process can

for example be designed according to the National Fire Protection Association (NFPA) 85: Boiler and Combustion Systems Hazards Code (2011), which is a code that sets "design, installation, operation, maintenance, and training" standards for "safe equipment operation" [23].

In NFPA 85 some requirements are stated. The purge shall for example be at least five volume changes and last for more than five minutes. Also, the mass flow during purge have to be at least 8 % of full power mass flow [23]. The purge time is calculated with equation (2.39) [24]. NFPA 85 is an American standard and the purge values can be changed depending on the site. When modelling in Dymola the purge speed level, time and other parameters can be set manually.

$$t_{purge} = n_p \cdot \left( \frac{V_{GT}}{\dot{V}_{purgeGT}} + \frac{V_{Exsys}}{\dot{V}_{purgeExsys}} \right) \quad (2.39)$$

### 2.16 Natural gas

Natural gas is a fossil fuel that was produced by nature millions of years ago. Just as coal and oil it consists of remains of plants and animals that have been transformed because of pressure and heat in layers deep down in the ground. The gas often occurs in natural pores in the bedrock and in coal deposits, which is called coal bed methane [25].

The natural gas contains mainly of methane (80 to 95 %), and small amounts of ethane and other hydrocarbons [26]. When analysing natural gas it is often defined as a dry gas, but in reality the gas is never free from liquids. Water condensate in the pipeline and liquids from the lubrication systems in pumping stations makes it a wet gas [4].

Transportation of natural gas is a great challenge. The gas is transported from producing areas to areas with high demand. The efficient and effective way to do this is with pipelines. The network of pipelines worldwide is huge and can cross whole countries, for example east-west pipeline in USA and Russia. Pump stations are placed in these networks to give the gas the pressure needed for transportation [27].

### 2.17 El-Encino

The El-Encino project is an ongoing Siemens project still under construction and it is used as a reference project in this thesis for verification and evaluation purposes. The site is located in Mexico and will be a part of the "La Laguna" pipeline that will run a total of 465 km between El-Encino and La Laguna. The compressor station, that Siemens has a vital role in constructing, will have three parallel compressor trains consisting of the

SGT-750 as the driving component and the STC-SV as the driven component. In this thesis the data used in the compressor system verification is retrieved from El-Encino.

### **2.17.1 SGT-750**

The SGT-750 is an industrial gas turbine with the weight advantages of an aero-derivative gas turbine and the robustness and flexibility of an industrial gas turbine. It was designed for long operating times and is easy to maintain and with a high availability and reliability. Because of the low downtimes for planned overhaul and maintenance the SGT-750 achieves a high availability which makes it useful both for PG but especially for MD purposes. SGT-750 is a twin-shaft axial gas turbine with a two stage free power turbine which delivers 41 MW in MD applications. The gas generator consists of an axial compressor with 13-stages and an overall pressure ratio of 24.3. The gas turbine compressor is driven by a two staged turbine which consists of an inlet stator with guide vanes where the first stage is cooled by both convective and film cooling. The SGT-750 has an efficiency of 40.3% for PG and 41.6 in MD applications and is suitable for both liquid and gaseous fuels [28].

### **2.17.2 STC-SV**

The compressor used in the El-Encino project is a compressor of the STC-SV series. The compressor is a single shafted centrifugal compressor with vertically split casing and there could be up to ten impellers in a single casing. The STC-SV is a diversified compressor that can be used in both standard and high-pressure applications. With its robust design it allows high nozzle loads and compression of gases with any molecular weight. The STC-SV is optimized for applications with low molecular weight and high pressure [29].

## **2.18 Tools**

### **2.18.1 Dymola**

The main software used in this report is the simulation and modeling tool Dymola, Dynamic Modeling Laboratory, which makes it possible to handle complex and integrated dynamic systems. The software is based on the Modelica language which is an object-oriented, declarative, multi-domain modeling language. Modelica uses equations to describe physical systems instead of algorithms which makes it easy to use and to understand. When the governing equations have been stated for a system, Dymola translates the equations into a code. Dymola has two modes in terms of modelling, the

text or code editor, and the graphical editor. The graphical editor in Dymola is a drag and drop editor in which it is possible to connect different parts into complex systems which is a convenient way to create models without having any deeper knowledge in the Modelica language. Dymola and the Modelica language offers the possibility to create new models from scratch, but also, there is the option of modifying existing models into the system by adding new code or new components to it. Except for the two modeling modes mentioned, Dymola also consists of a simulation mode. In the simulation mode the equations are solved and the user has the possibility to visualize the system by plotting the dynamic behaviour [30].

### **2.18.2 SVN/GITLab**

SVN and GITLab are two version management systems used at Siemens where updated Dymola models are checked in and made available for all employees. The system is global which make the models available from Siemens sites all over the world.

### **2.18.3 STA-RMS**

STA-RMS (Siemens Turbomachinery Applications - Remote Monitoring System) is a database consisting of raw data retrieved from all Siemens sites around the world. In RMS-View the user can study and download performance data from as late as the previous day for any machine active on site. The STA-RMS is used in this thesis to retrieve data for MD sites in order to verify the behaviour of the compressor train model.

### **2.18.4 WebPlotDigitizer**

WebPlotDigitizer is a tool used to extract numerical data out of plots and images. The tool can handle different kinds of 2-D plots and allows the user to calibrate the axes and then choose the points of interest in the plot. The data can then be exported to Excel for further use.

### **2.18.5 VLE Flash**

VLE Flash is a tool developed for the natural gas & petroleum industry by Flow Phase Inc. The tool calculates thermodynamic properties and draws phase envelopes and vapour fraction lines of different fluid mixtures which can be exported to Excel. The program consists of a database of 215 components, mostly hydrocarbons, and mixtures of up to 20 components can be studied [31].





# 3. Methodology

This section treats the different steps that have been carried out during the project. It provides information of how the compressor model was constructed and includes the assumptions and decisions that were made when modelling different components.

The first step of the project was to perform a literature study where reports and articles were reviewed. From this study the chapter Theory were created. The literature study is represented in the theory section. Equations and methods on how a compressor system could be modelled were found in the literature and created a base for the compressor model and auxiliary systems. The compressor system was modelled in Dymola part by part in order to ensure stability of the system. When the model fulfilled the specifications and requirements needed, the model was implemented by connecting it to the existing Dymola model of the SGT-750.

## 3.1 Literature study

During the first steps of the literature study available literature were reviewed and categorized according to topic and relevance. The literature was both internal within Siemens and external. The categorizing system made it easy to retrieve literature later in the project and find information about a specific topic. By doing this the literature study were performed continuously during the project as new components were modelled.

The literature study gave basic knowledge related to the project, such as governing equations and information about auxiliary systems as valves and control systems. By looking at similar projects the set-up for the simulation could be optimized to give the best result.

## 3.2 Dymola model of compressor system

During the years SIT engineers have designed their own Dymola Model Library, containing several basic models that can be used in more complex systems. These represent a variety of components and are specially designed to fit the company's applications well. Some examples of modelled components are valves, pipes and compressors. When designing the compressor train in this project these basic models often represent a platform to start from, even though many components are designed from scratch.

The compressor system was modelled as the first part of this project and consists of a number of components, which can be seen in Figure 3.1 below. The components will be described further in the following sections.

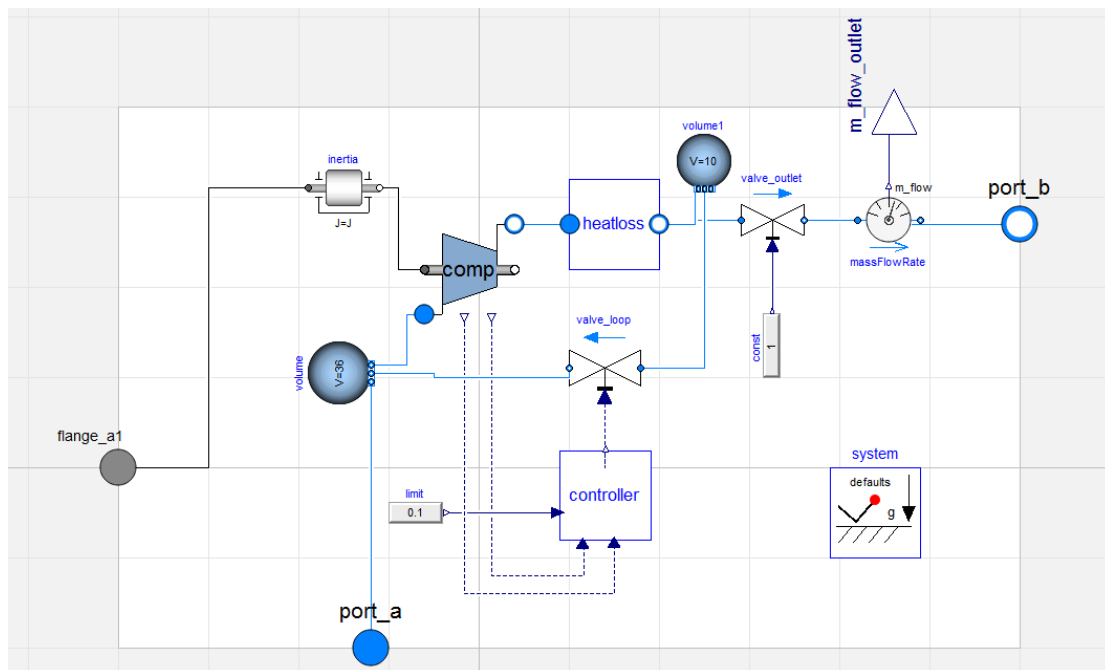


Figure 3.1: The compressor system modelled in Dymola.

### 3.2.1 Compressor

The compressor modelled in this thesis is based upon the existing basic compressor model developed by Siemens, with features rebuilt for the specific application. This section describes how the basic model is constructed and how it has been adjusted in this thesis.

#### 3.2.1.1 Basic Model

The basic model developed by Siemens is a thermodynamic compressor model based on characteristics. The model uses three governing equations to describe the behaviour of the compressor, the energy balance, the mass balance and the substance mass balance. These can be written as equation (3.1), (3.2) and (3.3) respectively.

$$E_{in} - E_{out} = \Delta E_{system} \quad (3.1)$$

$$\dot{m}_{in} - \dot{m}_{out} = \Delta \dot{m}_{system} \quad (3.2)$$

$$\dot{m}_{X_i,in} - \dot{m}_{X_i,out} = \Delta \dot{m}_{X_i,system} \quad (3.3)$$

The process is assumed in the model to be adiabatic, continuous and with constant mass fractions which changes the above equations to:

$$W_{in} + \dot{m}(\Delta h) = 0 \quad (3.4)$$

$$\dot{m}_{in} - \dot{m}_{out} = 0 \quad (3.5)$$

$$\dot{m}_{X_i,in} - \dot{m}_{X_i,out} = 0. \quad (3.6)$$

To calculate variables of interest the basic model make use of control volumes described in section 2.2 Compressor. It also uses the ideal gas model according to 2.5 Ideal gas model. The medium in the model consists of different substances and retrieves base properties as enthalpy, entropy, inner energy and molar mass by using the ideal gas data based on NASA Glenn coefficients. It is a library containing thermodynamic data for over 2000 solid, liquid and gaseous species for temperatures between 200 and 20000 K. The NASA Glenn coefficients will not be further described in this thesis but can be studied in [32].

#### 3.2.1.2 Characteristics

The compressor characteristics implemented in the model differs from the characteristics described in 2.8 Compressor characteristics. The characteristics is visualized in Figure 3.2, where the x-axis is standard volume flow, the y-axis is discharge pressure and instead of isentropic efficiency the discharge temperature is plotted in the characteristics as the blue

lines. The normalized speed is still the fixed parameter as described in [2.8 Compressor characteristics](#). A single map covers only the performance at a specific compressor inlet pressure. In MD applications the inlet pressure to a compressor train varies which is why two maps as the one in [Figure 3.2](#) for different inlet pressures were implemented in the model to increase the accuracy.

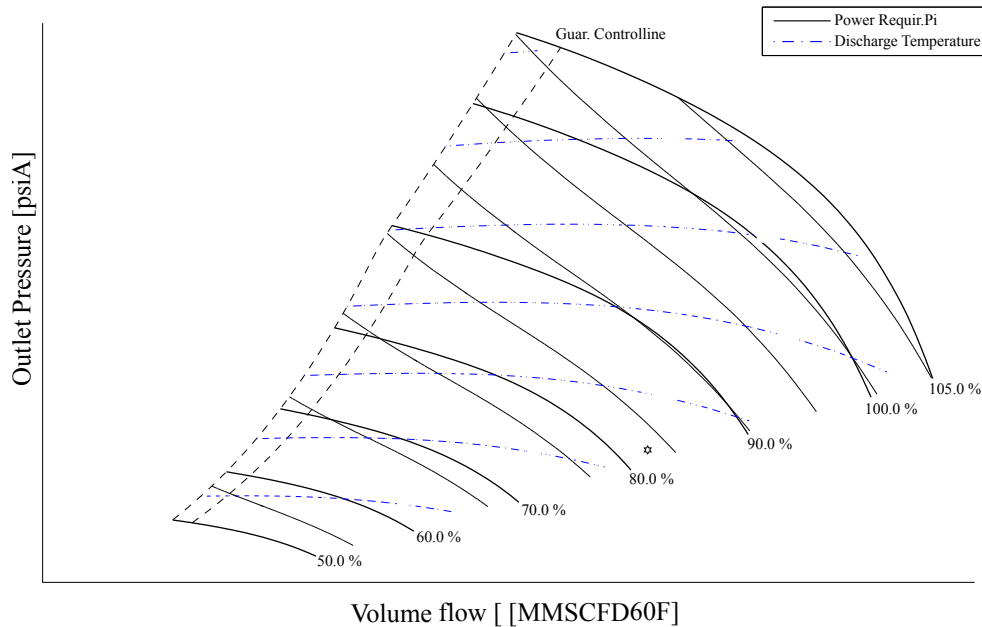


**Figure 3.2: The compressor characteristics used in the model. The volume flow given in MMSCFD60F (million standard cubic feet per day at 60 Fahrenheit and 1 bar) and the pressure in PsiA. The straight lines represent the power needed and the dotted ones represent the discharge temperature.**

The compressor maps were added to the model through reading of the values in the actual map, due to values not being available in table form. The pressure and volume flow were added with the program WebPlotDigitizer and the temperatures were estimated by hand. Since the compressor maps are created down to 50% of nominal speed the lower speeds had to be extended by hand and manually put in to the Dymola code. The maps are used in the model as a sequence of inter- and extrapolation depending on the actual conditions. These are performed in 3D between different inlet pressure maps, in 2D between speed lines and in 1D on the actual speed line. Inputs to the characteristics are inlet pressure, rotational speed and discharge pressure. The outputs are volume flow, surge factor and discharge temperature, which can be seen in [Figure 3.3](#) below. The volume flow is converted to mass flow in the model with a reference density at pressure

and temperature of 1 bar and 60 °F. The Variable Guide Vane input to the compressor map is not used in this project due to limitations, however it is still in the model due to the fact that it could be used in future models at Siemens.

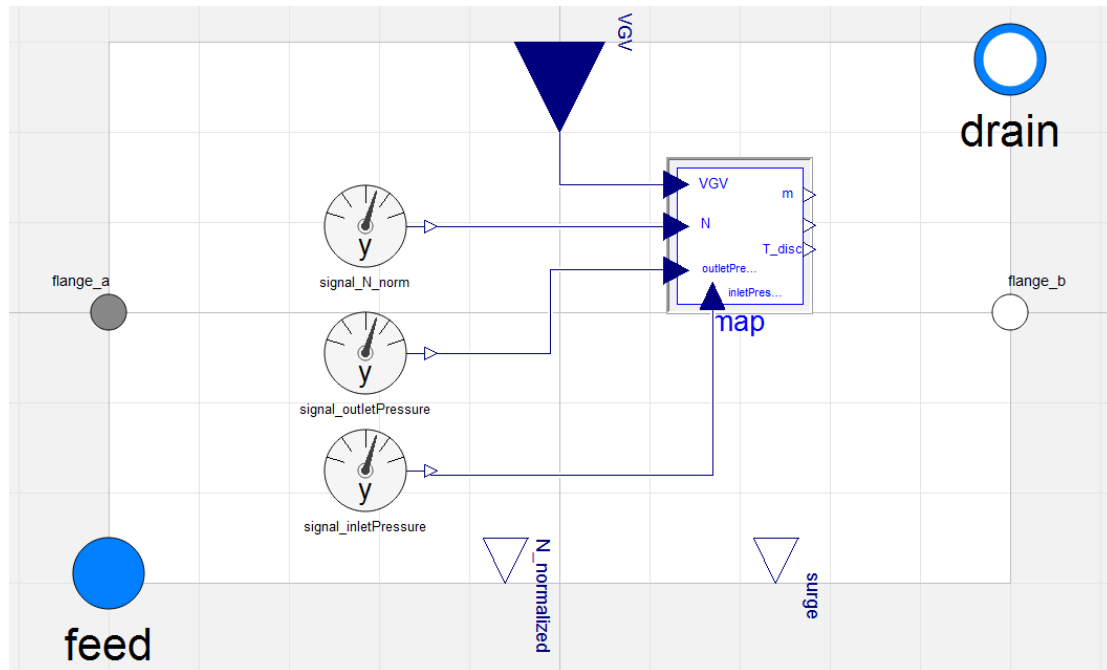


**Figure 3.3: The Dymola model of the compressor.**

### 3.2.2 Medium

The medium in the compressor model in Dymola was created according to the natural gas specified in the El-Encino project. The gas composition can be seen in Table 3.1.

### 3.2.3 Compressibility

In this report the medium to compress was natural gas, that mainly consist of methane. The parameters for methane is given in Table 3.2. In this report the pressure is in the range [50, 80] bar and [289, 373] K, which gives a  $p_R$  in the range of [1.09, 1.74] and  $T_R$  in the range of [1.51, 1.95]. By using Figure 2.5 it can be found that the four combinations of  $p_R$  and  $T_R$  gives a  $Z$  of  $Z_1 = 0.9$ ,  $Z_2 = 0.97$ ,  $Z_3 = 0.85$  and  $Z_4 = 0.95$ . That means that in the worst case scenario  $Z = 0.85$ . In the modelling it only affects the calculation of density and inner energy, but does not change the value of the reference medium when converting between units (from MMSCFD60F to  $\text{kg s}^{-1}$ ). The reference medium has a pressure of 1 bar and temperature of 60 °F which gives  $Z = 1$ . The result of this is that  $Z$  will not affect the calculations or result in a significant way. In the

**Table 3.1: Composition of the Natural Gas in the model.**

| Substance     | $M$ [kg/kmol] | $Mol\%$ |
|---------------|---------------|---------|
| Methane       | 16.04         | 93.665  |
| Oxygen        | 32.00         | 0.149   |
| Carbondioxide | 44.01         | 0.955   |
| Nitrogen      | 28.02         | 0.149   |
| Water         | 18.02         | 0       |
| Ethane        | 30.07         | 4.815   |
| Propane       | 44.09         | 0.218   |
| n-Butane      | 58.12         | 0.02    |
| Isobutane     | 58.12         | 0.021   |
| n-Pentane     | 72.15         | 0.002   |
| Isopentane    | 72.15         | 0.003   |
| n-Hexane      | 86.17         | 0.003   |

original Dymola functions the gas is handled as an ideal gas with a compressibility factor equal to 1. Due to that, the  $Z$ -value was added as a parameter in the compressor and in the medium for future development of the model.

**Table 3.2: Equations for gas properties. Table: [12]**

| Substance                | $M$ [kg/kmol] | $R$ [kJ/kgK] | $p_R$ [MPa] | $T_R$ [K] |
|--------------------------|---------------|--------------|-------------|-----------|
| Methane, CH <sub>4</sub> | 16.04         | 0.518        | 4.6         | 191       |

### 3.2.4 Anti-surge loop

The compressor system in this project is equipped with an anti-surge loop. This loop consists of a control valve that is controlled by a control system. The purpose of the loop is to avoid surge in the compressor, and its components are further described in following sections.

#### 3.2.4.1 Control valve

The anti-surge valve is one of two valves used in the compressor model in order to control the flow. The characteristic of the valve was set as linear which means that 10 % opening gives a 10 % flow of maximum [12]. The valve was designed according to specifications of the El-Encino project and have a  $K_v$  value of 1650. The  $K_v$  is known as the flow



### 3.2.5 Check valve

A check valve was modelled at the outlet to prevent reversed flow from the downstream pipeline. An example of a check valve is the swing valve, as can be seen in Figure 3.5. Unlike the control valve the check valve is either totally open or totally closed and do not have to be controlled in the same extent as the control valve, thus no control system is modelled for this component. Despite this, all types of check valves acts differently and they all got unique characteristics [12].

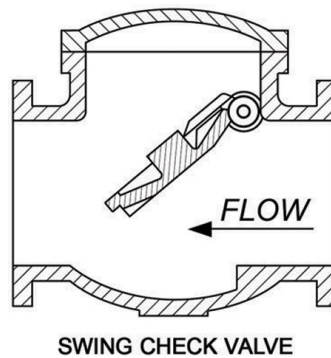


Figure 3.5: Swing check valve. (Figure: [33])

### 3.2.6 Cooler

According to equation (2.23) the pressure rise contributes to a temperature rise of the medium. Because of the surrounding circumstances it is required to maintain a low temperature of the medium, 16 °C. This applies to the outlet of the system, but also to the anti-surge loop. During start-up the recycling valve will be open, and without a cooler the temperature in the loop would increase successively. For this reason the cooler was placed after the compressor.

The task of a standard cooler is to exchange heat between mediums. Figure 3.6 shows an example of a cooler, a Shell-and-Tube heat exchanger. One fluid is passing in the tubes, one in the surrounding shell and heat is transferred between them. The larger temperature difference and heat transfer area in the exchanger, the larger amount of heat is transferred [12]. However, the heat exchanger in this project was not modelled as a standard heat exchanger. Instead it was modelled as a simplification where the outlet temperature was set to 16 °C and the transferred heat flow,  $\dot{Q}$ , was added to the energy balance according to equation (3.7). By doing this the heat exchanger does not need any cold medium or any controlling of the cooler outlet temperature.

$$\dot{m}(\Delta h) - \dot{Q} = 0 \quad (3.7)$$



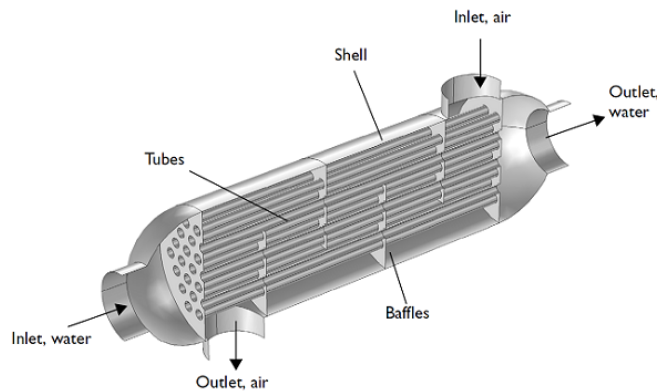


**Figure 3.6: Example of a Shell-and-Tube heat exchanger. (Figure: [34])**

#### 3.2.7 Source, Sink and Volumes

A source and a sink were also added in the model. They represent the upstream and downstream of the pipeline and can be seen as an infinitely large volume containing natural gas. In order for the system to be dynamic volumes had to be added as well. The values of the volumes were set according to the El-Encino case and represent the volumes of piping between components, and the components themselves.

#### 3.2.8 Ideal gas model

When the verification of the compressor system was performed it was noticed that Dymola only handles ideal gases, therefore an investigation of how this affects the accuracy of the model were performed. The main issue were the inaccurate enthalpy calculation performed by Dymola. It was investigated if Dymola only calculates the enthalpy with respect to temperature. The enthalpy for the main substance, Methane at 48 °C, was retrieved from [35] and compared with the enthalpy from Dymola. The software VLE Flash was used to calculate the enthalpy for natural gas treated as a real gas at the same operation points as in the verification of the compressor system.

### 3.3 Dymola model of gas turbine control system

To be able to run a gas turbine in a correct manner, all turbines are equipped with a control system. This system has three fundamental functions: start-up and shutdown sequencing, steady-state control during operation and protection of the gas turbine [4]. When using a gas turbine in an MD application instead of a PG application the control system had to be modified. In general the control system looks the same, but some components were added or replaced. This will be further described in the respective

section. Unless the opposite is stated, the controller works in the same way for both applications.

There are two main types of control systems - closed or open loop system. The open system induces a control signal for the system without any measurements. The closed system is controlled with a measured signal from the system itself. By calculating the deviation between the measured signal and a set point, the control signal can be changed [4].

The control system for the SGT-750 mainly consists of closed loops and contains many controllers who together control different parameters and values of the gas turbine. They all have their own tasks and limits, for example one controller controls the gas generator speed which has a maximum value and another controls the speed of the power turbine. The controllers are activated automatically when they are closest to its limit and then assume control of the operation. In the SGT-750 control system there are many different controllers, but in this report only the ones that are vital for this project are mentioned. Figure 3.7 shows a graphic view of the controllers in Dymola. The three controllers in the MD box were the ones modelled in this project and during MD operation the FLC controller was deactivated to ensure the right control of the gas turbine.

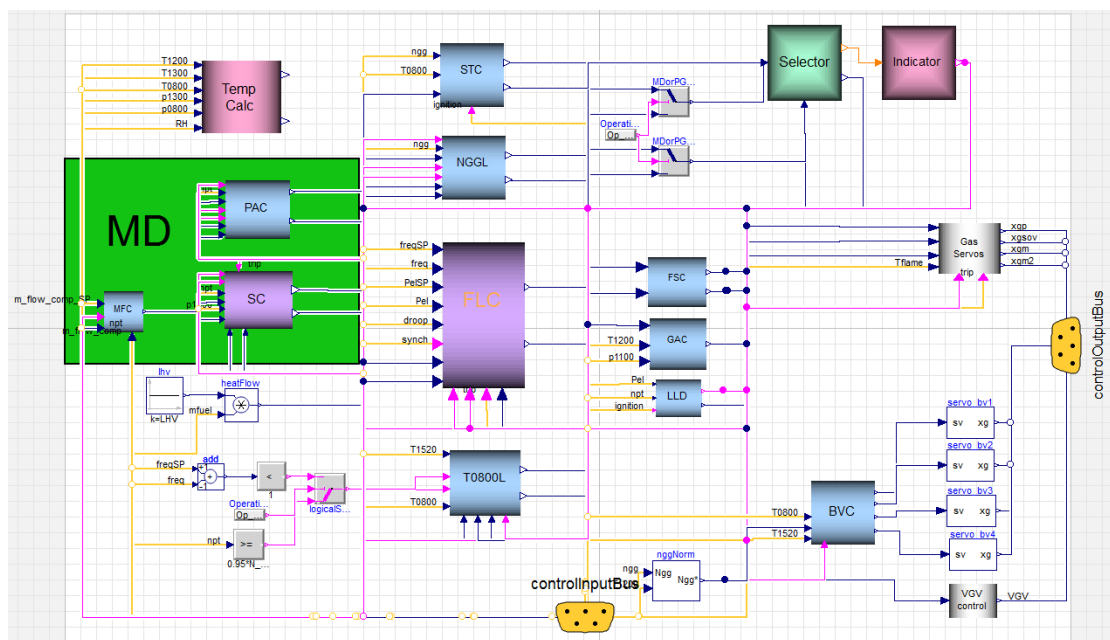


**Figure 3.7: The modelled control system for SGT-750. The controllers in the green box are specially designed for MD applications.**

### 3.3.1 Starter motor

The starter motor has two main purposes: to drive the gas turbine through a purge process and to accelerate the gas generator up to a speed where it got enough mass flow to provide itself with power. The starter motor is an electrical engine and its size depends on the type and size of gas turbine.

### 3.3.2 Start controller - STC

The start controller is the first controller to take over from the starter motor during start-up. When chosen rotational speed is reached the STC starts the ignition and then activates a fuel ramp to the burner which causes the firing temperature to rise and the gas generator to accelerate. The purpose of the STC is to get good starting reliability and to avoid engine damage. By limiting the rotor acceleration, the STC prevents too high thermal stress of the turbine. The STC is active until the gas generator reaches a certain speed, around half way through the acceleration, where NGGL takes over the operation, see section [3.3.3 Gas generator speed limiter - NGGL](#) [24].

### 3.3.3 Gas generator speed limiter - NGGL

When the NGGL is in operation it uses a PID-controller to accelerate the gas generator with a constant ramp. The value of the ramp changes at a certain speed. The controller limits the gas generator speed to avoid engine damage. For a PG application the NGGL is active until operation speed is reached, which is when the generator has the same frequency as the grid (50 Hz in Sweden). Though, for an MD application NGGL is active until just before min. continuous speed is reached, which depends on the operation situation [24].

### 3.3.4 Power turbine acceleration controller - PAC

This was the first controller modelled in this project. For an MD application it is more important to have a PAC which limits the acceleration of the PT, because of its lower inertia. A too high acceleration can damage the power turbine. The feedback for PID-controller in the PAC is the derivative of the PT speed, which is limited to a given value [24]. If the PAC is active it gives the power turbine speed this constant derivative. The PAC is active during start-up and up to a set point close to the min. continuous speed, just as NGGL. This means that PAC is active at the same time as both STC and NGGL. The design of the PAC can be seen in [Figure 3.8](#).

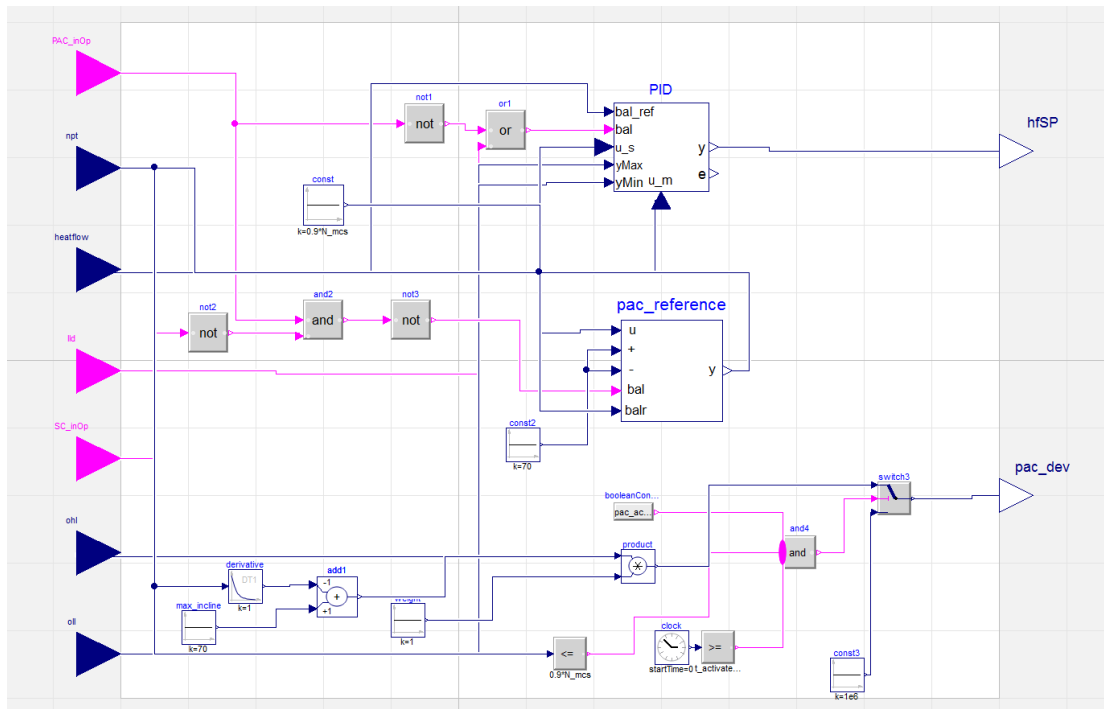


Figure 3.8: Dymola design of PAC - power turbine acceleration controller

### 3.3.5 Frequency and load controller/Speed controller - FLC/SC

In PG applications the FLC is active until idle speed is reached during start-up. It can be set to either frequency control or load control depending on the situation. In this project the FLC is inactive and replaced with the SC. The SC takes over from NGGL and PAC during start-up just before min. continuous speed. It uses a PID controller to keep the PT speed at a required level. Even if the controller focus on the speed, the power turbine acceleration is limited due to a table in [24]. This table give loading restrictions in  $rpms^{-1}$  based on gas turbine compressor discharge pressure. The design of the SC can be seen in Figure 3.9.

### 3.3.6 Mass flow controller - MFC

Even if the SC controls the PT speed (and thereby the speed of the driven component), it is not practical for the operator to control the gas turbine in such a way. That is why it often is advantageous to add another controller. In this project it was desirable to control the system on mass flow through the driven compressor, which is why the MFC was modelled. The MFC uses a PID controller to control the PT speed by measuring the deviation of the actual mass flow and the mass flow set point. The model was designed so that the user easily can deactivate the MFC controller and use the SC instead. The design of the MFC can be seen in Figure 3.10.

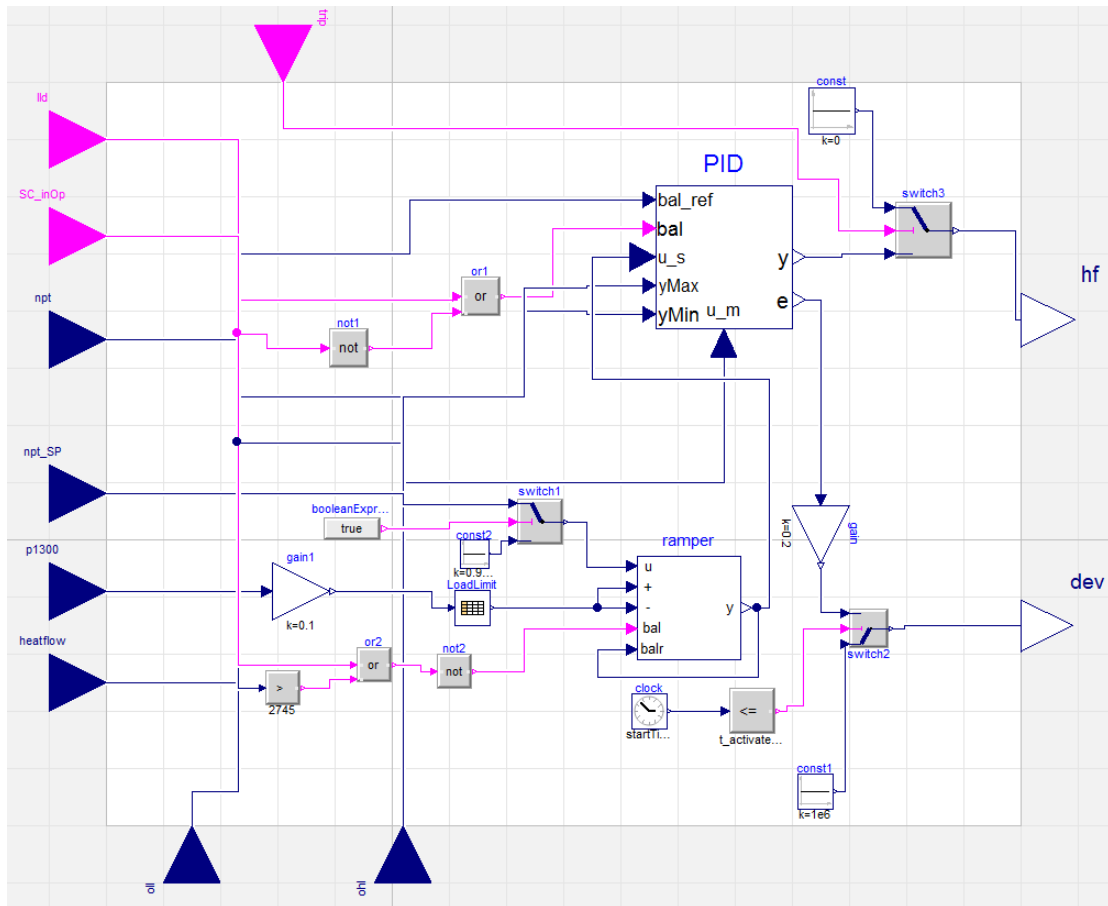


**Figure 3.9: Dymola design of SC - Speed controller**

#### 3.3.7 Exhaust temperature limiter - T0800L

At full load operation the T0800L controller limits the exhaust temperature,  $T_{0800}$ . The purpose of this is to limit the turbine inlet temperature,  $TIT$ , due to material characteristics [24]. The controller measures both  $TIT$  and  $T_{0800}$  and compares them with their maximum values.

#### 3.3.8 Load loss detection - LLD

The purpose of the LLD is to have a high sensibility when instant load drops occur. If one should occur the LLD reduces the fuel down to flame sustain level and opens the bleed valves according to a prescribed table [24]. This controller is not modified in this project.

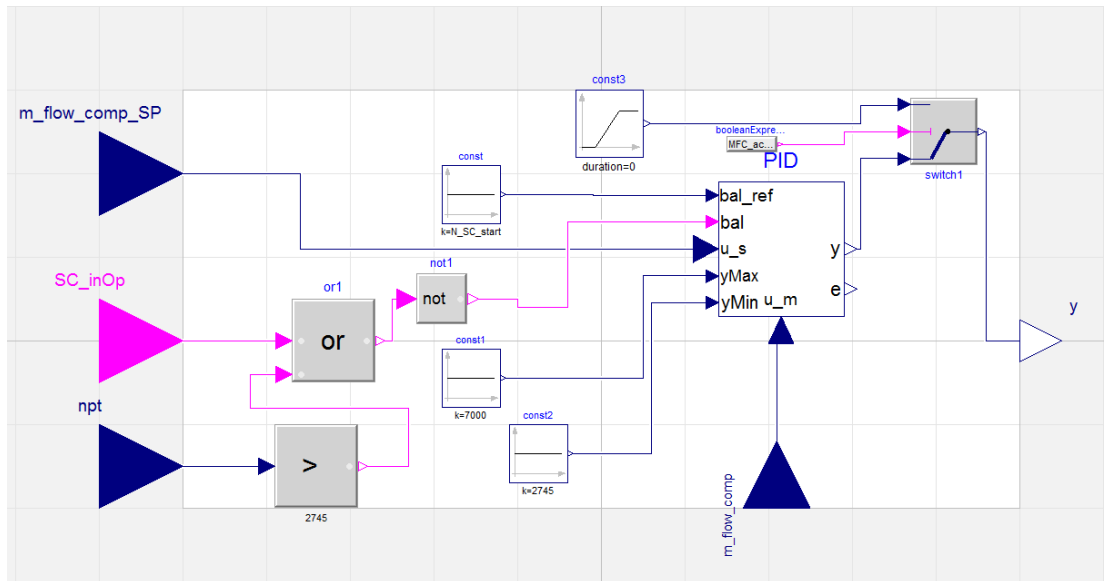


**Figure 3.10: Dymola design of MFC - mass flow controller**

### 3.3.9 Gas generator acceleration control - GAC

The GAC controls the upper limit of the fuel flow to avoid overheating and compressor surge. The fuel flow limit is set by the actual normalized compressor speed [24]. This controller is not modified in this project.

### 3.3.10 Flame sustain control - FSC

This controller is very important and gives a lower limit of the fuel flow. This limit is the lowest possible flow to sustain the flame, though the other controllers can call for a fuel flow below this. In case of a flameout the flame has to be re-lit, which takes time and is bad for the performance [24]. This controller is not modified in this project.

### 3.3.11 Gas generator deceleration control - GDC

The GDC is also used to avoid flameout, it controls the minimum fuel flow based on the normalized gas generator speed. The lower limit is also depending on PG or MD. For an MD application the lower limit is increased with required fuel flow to match load at minimum PT speed [24]. This controller is not modified in this project.

### **3.3.12 Bleed valve controller - BVC**

The BVC controls the compressor bleeds, that are used to lead away some of the air in the gas turbine compressor. This is done to manage differences in stage compression caused by speed variations. This allows the compressor stage to operate at low speeds without stalling, because of choked subsequent stages [24]. This controller is not modified in this project.

## **3.4 Implementation - Connecting the compressor system with the SGT-750**

One of the main objectives in this project was to connect the compressor model with the existing SGT-750 model at Siemens and then simulate a starting sequence. In order to achieve this several changes had to be made in the SGT-750 model. The SGT-750 model were previously built to simulate dynamic behaviour during PG and therefore had to be adapted to the MD application. The compressor model and the modified SGT-750 model can be seen in the Figure 3.11 below. The features including the frequency of the generator had to be changed to power turbine speed in order to be able to control the compressor train in a correct manner. New controllers were added to the SGT-750 controller which has been described in the previous sections.

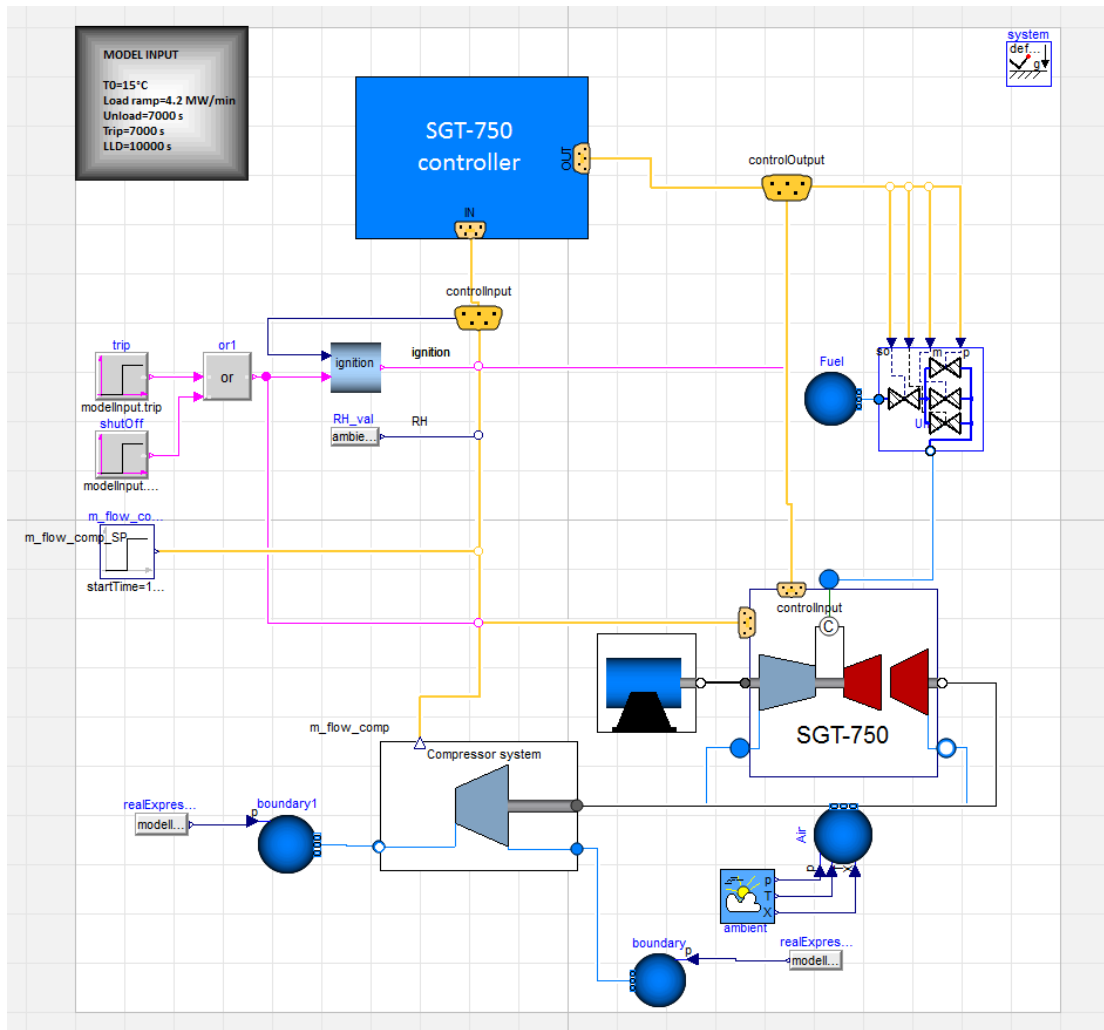


Figure 3.11: The SGT-750 system connected with the compressor system.



## 4. Verification and analysis

To be able to analyse the gas turbine behaviour in a MD application one have to ensure that the thermodynamic model corresponds to reality. This is done with the verification process presented in this chapter. The verification is visualized in normalized graphs due to company secrecy. The graphs were normalized with the final or maximum value for the studied sequences. The verification was divided into two sections. Firstly the verification of the compressor model was performed, with data from the compressor manufacturer. Secondly, when the compressor system and the gas turbine were connected into a compressor train, the entire compressor train's performance was verified in three steps that will be further described in the current section.

### 4.1 Verification of the compressor system

As a part of the verification of the compressor system, simulations were performed at two steady state operation points with the purpose of verifying the compressor. The chosen points represent two scenarios from two different compressor maps, i.e. different compressor inlet pressures. The results of the simulations were compared with data sheets from the compressor manufacturer. The deviation for each parameter was calculated with equation (4.1), where  $X_{simulation}$  is the parameter value from the simulation and  $X_{data}$  is the given parameter value from the compressor manufacturer. The average deviation of the two scenarios was calculated with equation (4.2) where  $X_1$  is the deviation from one scenario and  $X_2$  from the other.

$$\text{deviation} = \left( \frac{X_{simulation}}{X_{data}} - 1 \right) \cdot 100 \quad (4.1)$$

$$\text{average deviation} = \frac{X_1 + X_2}{2} \quad (4.2)$$

Parameters that were compared with the data sheet were inlet volume flow, compressor outlet temperature, polytropic efficiency, power and polytropic head. The volume flow

and temperature were retrieved in the model as outputs from the compressor map, the polytropic efficiency was calculated according to [2.10 Polytropic efficiency using the sT-method](#), the power according to equation (4.3) and the polytropic head as equation (4.4). The polytropic head denotes the amount of work required per kilogram of compressed gas.

$$P = \Delta h \cdot \dot{m} \quad (4.3)$$

$$\text{Head}_{poly} = Z_{naturalgas} \cdot R_{inlet} \cdot T_{inlet} \cdot \frac{\gamma_{inlet}}{\gamma_{inlet} - 1} \left( \frac{p_{outlet}}{p_{inlet}}^{\frac{\gamma_{inlet}-1}{\gamma_{inlet}}} - 1 \right) \quad (4.4)$$

The anti-surge loop was an important part to verify when verifying the compressor system. Focus were on the control system of the control valve, i.e. to ensure that the surge margin were kept above the chosen limit and that the control system behaved as intended. Two different simulations were performed, a start-up and a steady state to verify both cases mentioned in [3.2.4.2 Control system](#). During the verification the anti-surge loop control system was tuned in, in order to keep a steady and accurate control of the surge margin.

#### 4.1.1 Compressor verification

To verify the compressor, the two steady state operational points mentioned in [4.1 Verification of the compressor system](#), were simulated. The input data for the two scenarios can be seen in Table 4.1, under "Input". The deviation for each parameter was calculated with equation (4.1), and the average deviation was calculated with equation (4.2). The average deviations can be seen in Table 4.1 under "Avg. dev.".

**Table 4.1: Verification results for the compressor system. "2023" means "Scenario 1A, 2023, 1 train" and "2024" means "Scenario 1A, 2024, 1 train". SI-units are not used since the data sheets from manufacturer were in American units.**

| Input                        |        |        | Output                                 |               |
|------------------------------|--------|--------|--|---------------|
| Parameter                    | 2023   | 2024   | Parameter                              | Avg. dev. [%] |
| Inlet pressure [psiA]        | 733.7  | 799.4  | Inlet volume flow [MMSCFD60F]          | 0.1           |
| Outlet pressure [psiA]       | 1025.2 | 1131.5 | Comp. outlet T [°C]                    | 1.6           |
| Comp. inlet T [°C]           | 16     | 16     | Polytropic efficiency [%]              | 2.8           |
| Comp. rotational speed [rpm] | 4643   | 4828   | Power [kW]                             | 15            |
|                              |        |        | Polytropic head [kJ kg <sup>-1</sup> ] | 0.7           |

As can be seen in Table 4.1 the deviations in general can be considered small. The power has a larger deviation due to miscalculated enthalpy in Dymola. This phenomena is described in chapter 3.2.8 [Ideal gas model](#). As mentioned, the temperature was manually put into the model, which contributes to the deviation of the compressor outlet temperature and the polytropic efficiency.

### 4.1.2 The ideal gas model

The result of the ideal gas model investigation can be seen in Figure 4.1 and in Table 4.2. In Figure 4.1 the blue line represents the enthalpy retrieved from [35] and the red line the enthalpy calculated in Dymola for Methane. The enthalpies have different reference states which causes a greater difference between the lines in the figure. It can be seen that the enthalpy has a clear pressure dependency during circumstances with this high pressure. Table 4.2 shows that the average deviation of the power was decreased from 15 % to 3.72 % when using the real enthalpy instead of the enthalpy from Dymola. The enthalpies shown in the figure

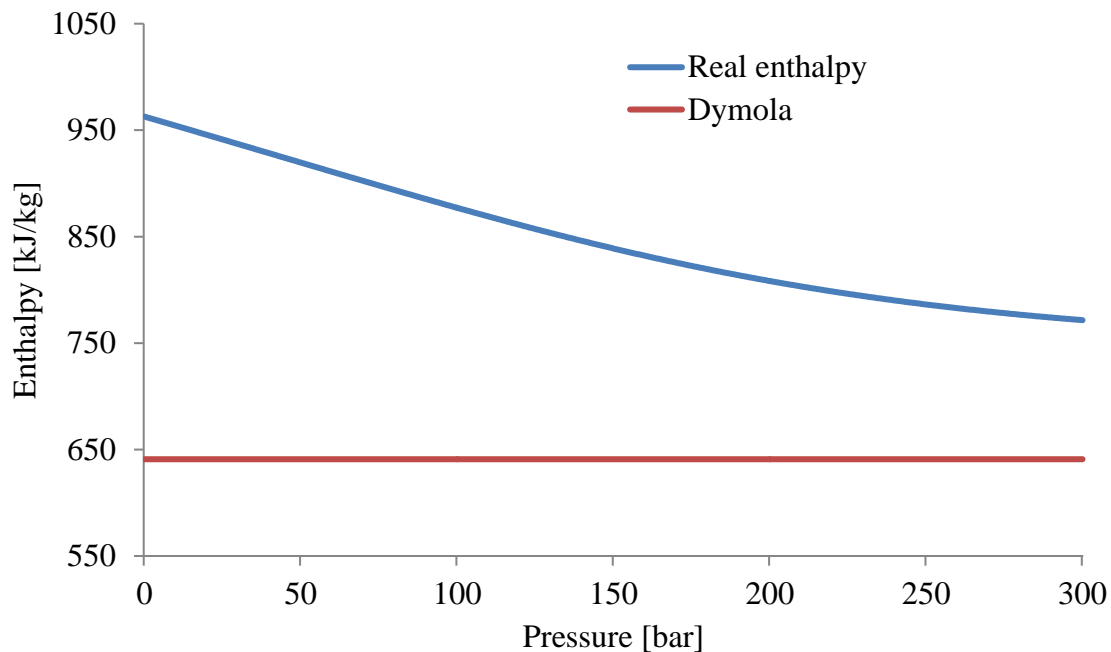


**Figure 4.1:** The figure shows the enthalpy retrieved from [35] and the enthalpy from Dymola for Methane as a function of pressure.

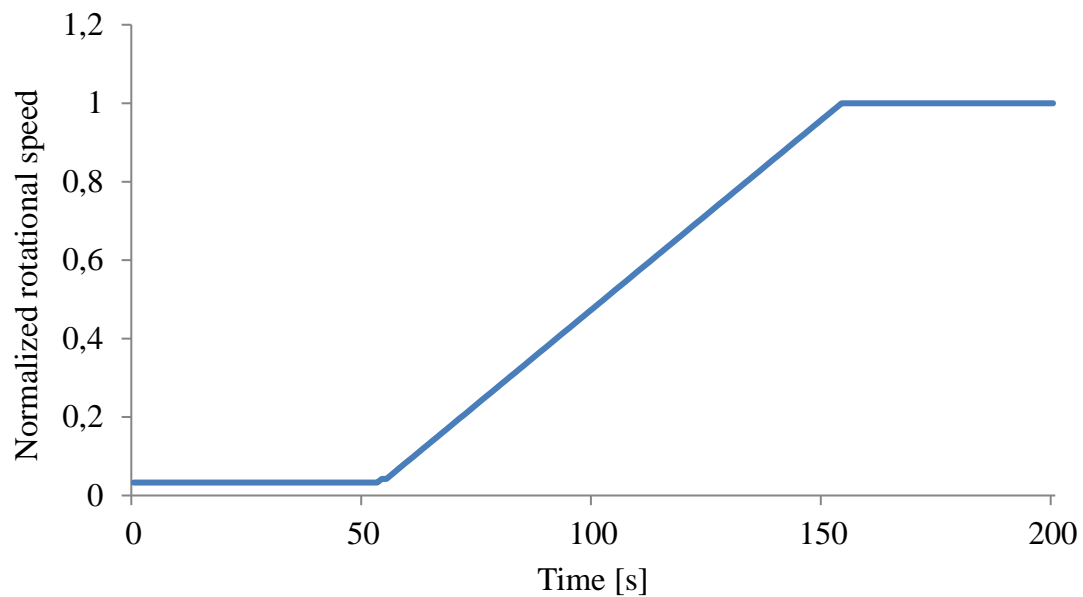
**Table 4.2:** Table showing the average deviation of the compressor power when using the enthalpy retrieved from VLE Flash for the two cases used in the verification of the compressor system. SI-units are not used since the data sheets from manufacturer were in American units.

| Case | $p_{comp. inlet}$<br>[psiA] | $p_{comp. outlet}$<br>[psiA] | $\Delta h$<br>[kJ/kg] | Dev<br>[%] | Avg. dev<br>[%] |
|------|-----------------------------|------------------------------|-----------------------|------------|-----------------|
| 2023 | 733.7                       | 1025.2                       | 63.75                 | 3.74       | 3.72            |
| 2024 | 799.4                       | 1131.5                       | 67.90                 | 3.71       |                 |

### 4.1.3 Start-up

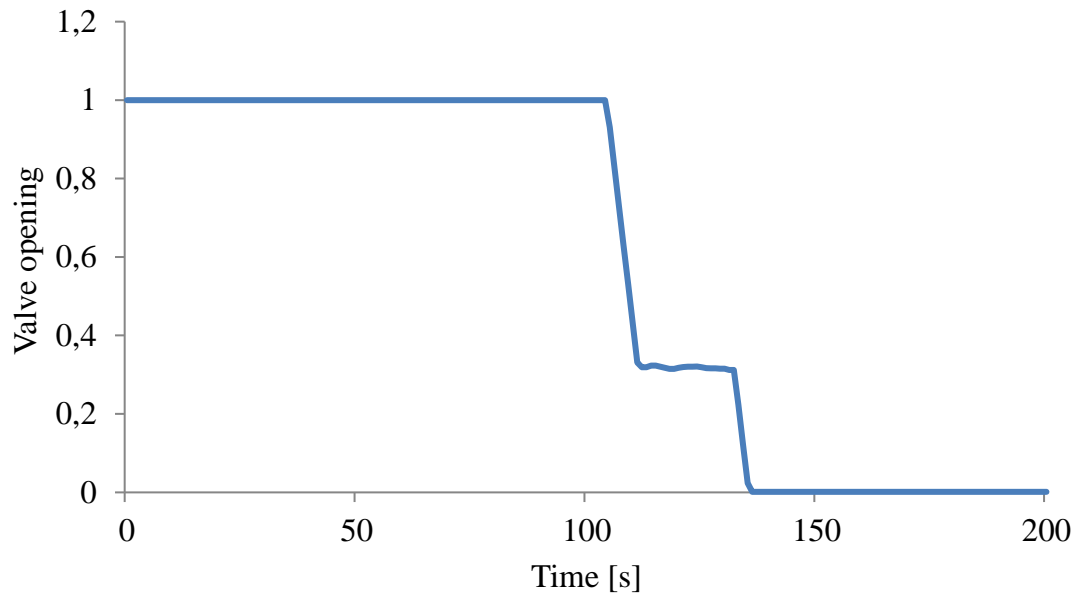
To verify the control system two different sequences were simulated, the first one was the start-up sequence.

Figure 4.2 shows the compressor speed during the start-up sequence, starting from almost zero rpm up to nominal speed of the compressor.



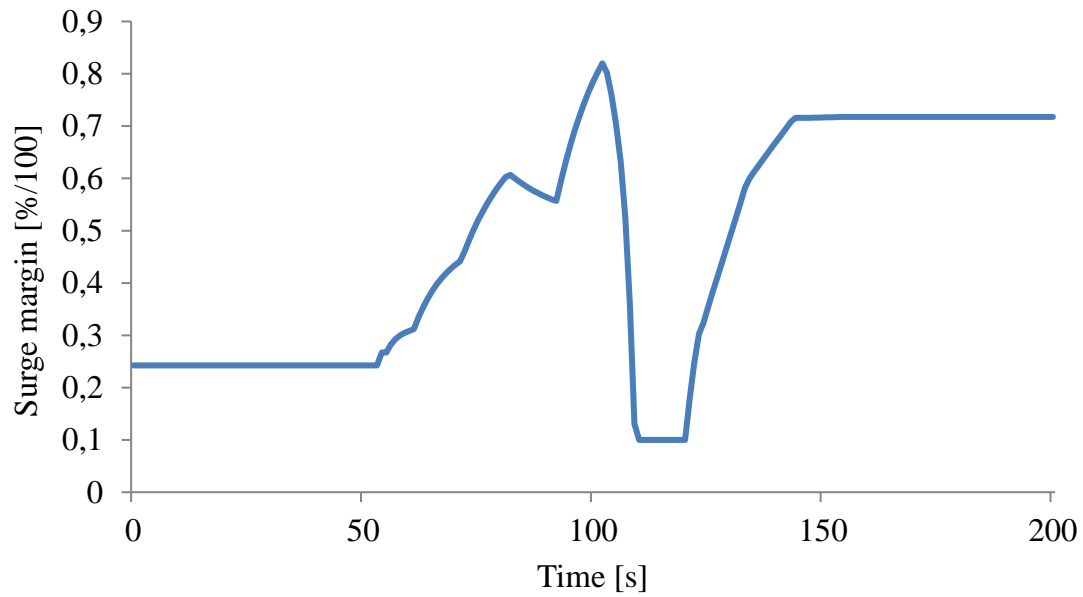
**Figure 4.2:** Compressor speed during start-up of the compressor system.

Figure 4.3 shows the opening level of the anti-surge valve during the start-up sequence. The valve follows the prescribed closing time according to [21].



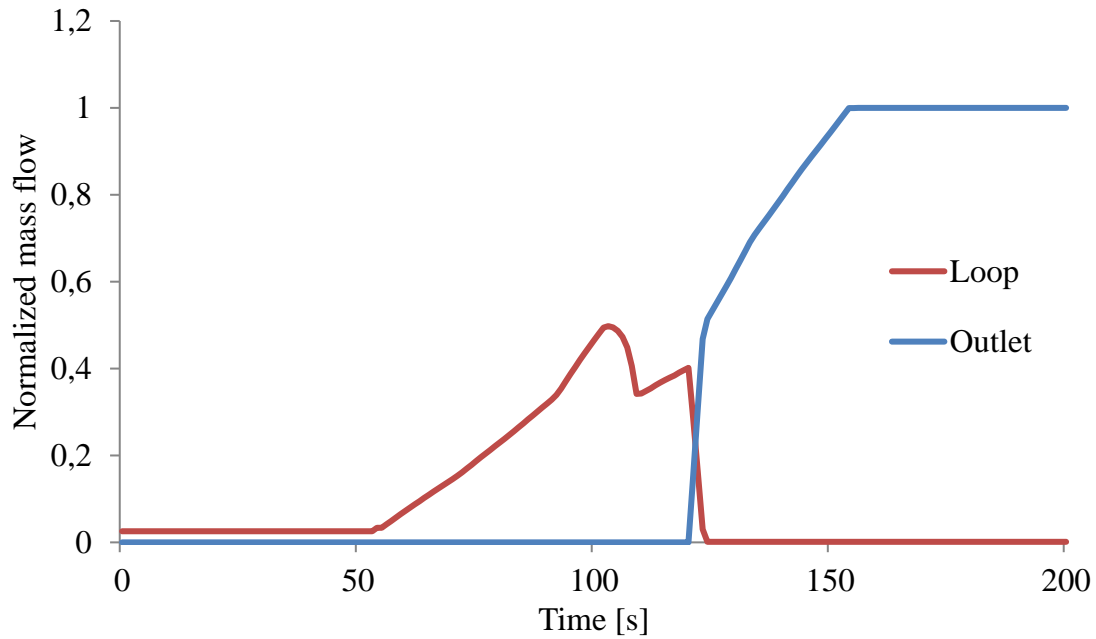
**Figure 4.3: Opening of the anti-surge valve during start-up of the compressor system.**

Figure 4.4 shows how the surge margin varies during a starting sequence. As the speed starts to increase the surge margin increases quite unevenly due to the inaccuracy of the map for speeds below the min. continuous speed. When this speed is reached the control valve starts to close as can be seen in Figure 4.3, and the surge margin decreases. When reaching 10 % the PI-controller keeps the margin at this limit and as the speed still increasing it will increase the mass flow, thus increase the surge margin.



**Figure 4.4: Surge margin during start-up of the compressor system.**

In Figure 4.5 the mass flow of the start-up sequence can be seen. As the speed increases, the mass flow increases. When reaching min. continuous speed the anti-surge valve closes and the mass flow through the loop decreases. Since the pressure is still below the back pressure in the sink the mass flow in the loop is the same as through the compressor. As the valve closes entirely the outlet mass flow increases when the back pressure is reached.



**Figure 4.5: Loop and outlet mass flow during start-up of the compressor system.**

The pressure have a clear dependency of the opening of the anti-surge valve which can be seen in Figure 4.6. As speed is increasing a small amount of pressure is building up, but as the valve closes pressure starts to build up rapidly. In order to reach a discharge pressure higher than the sink pressure the valve closes as much as it is allowed during start-up of the compressor system.

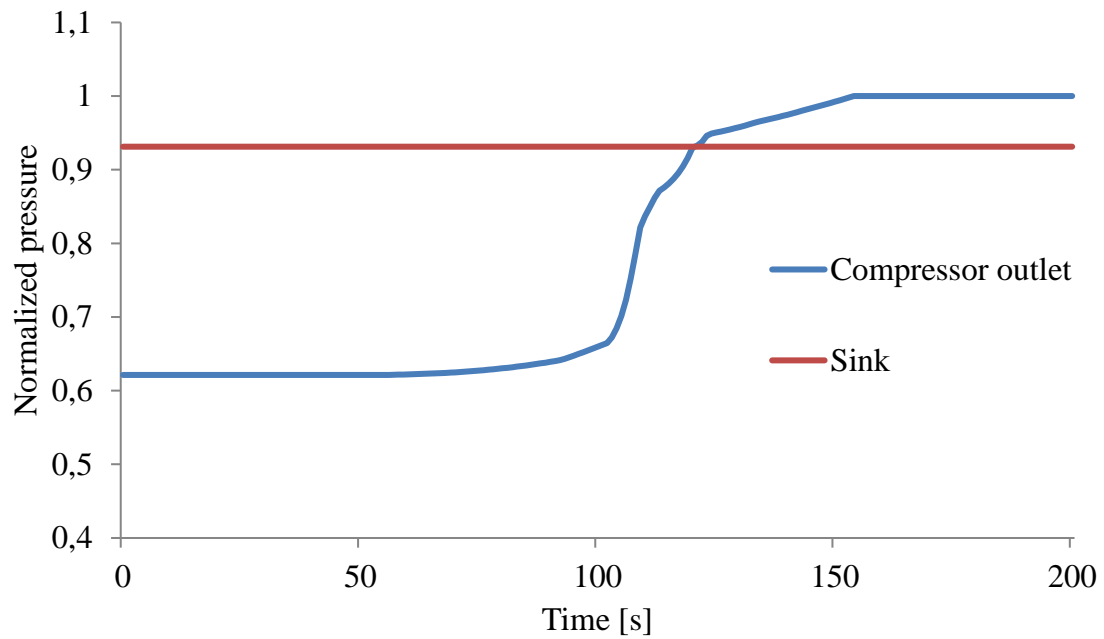


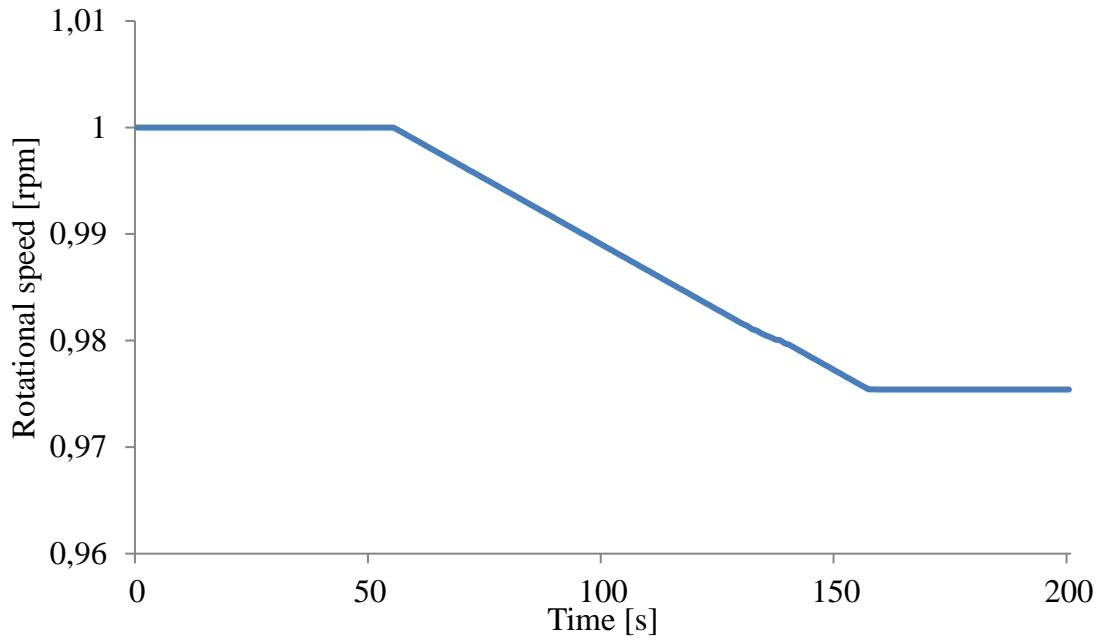
**Figure 4.6: Outlet and sink pressure during start-up of the compressor system.**

#### 4.1.4 Steady state

A steady state case was simulated as a negative ramp of the rotational speed in order to verify that the anti-surge loop control system starts to act when the surge limit is reached.

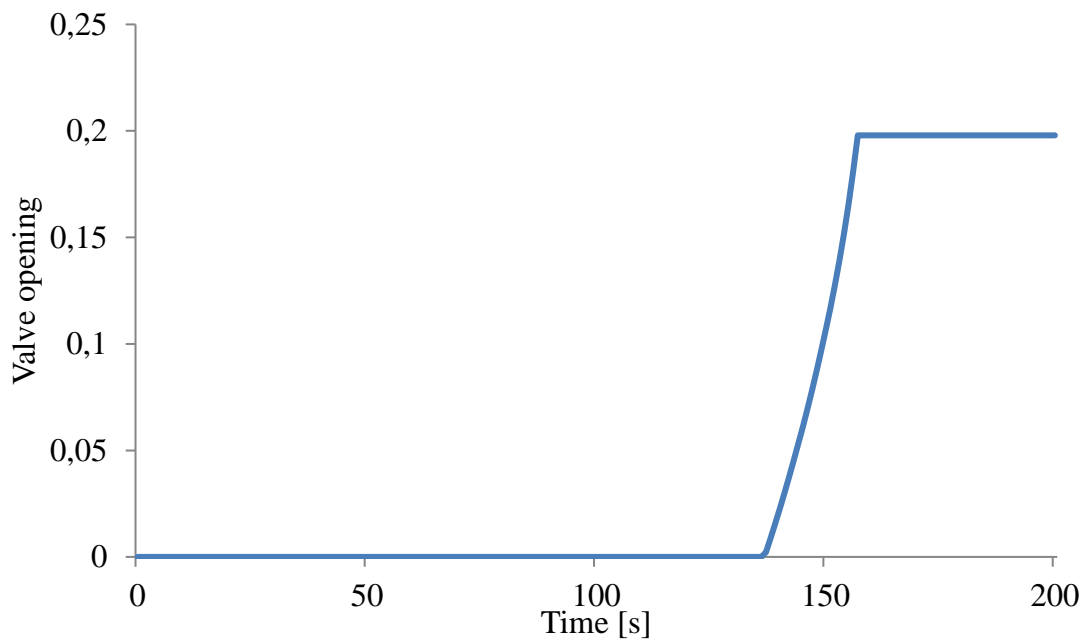
Figure 4.7 shows the speed ramp for the steady-state simulation, going from full speed down to 97.5 %.



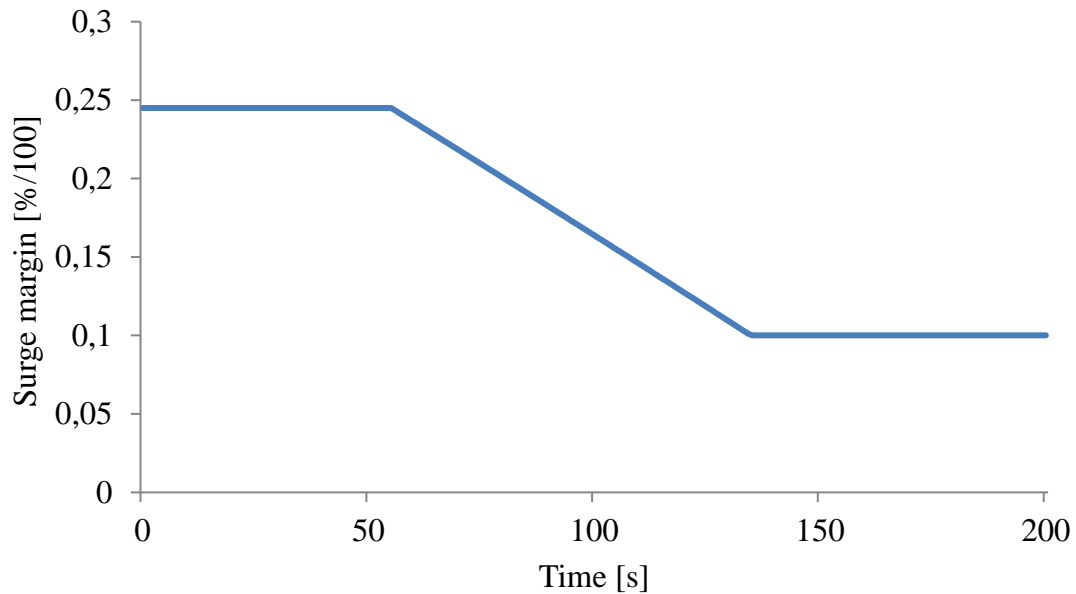


**Figure 4.7: Compressor speed during the steady state sequence.**

Figure 4.8 shows the opening of the anti-surge valve during the steady state sequence. The control of the valve shows no indications of oscillations or unsteady behaviour.



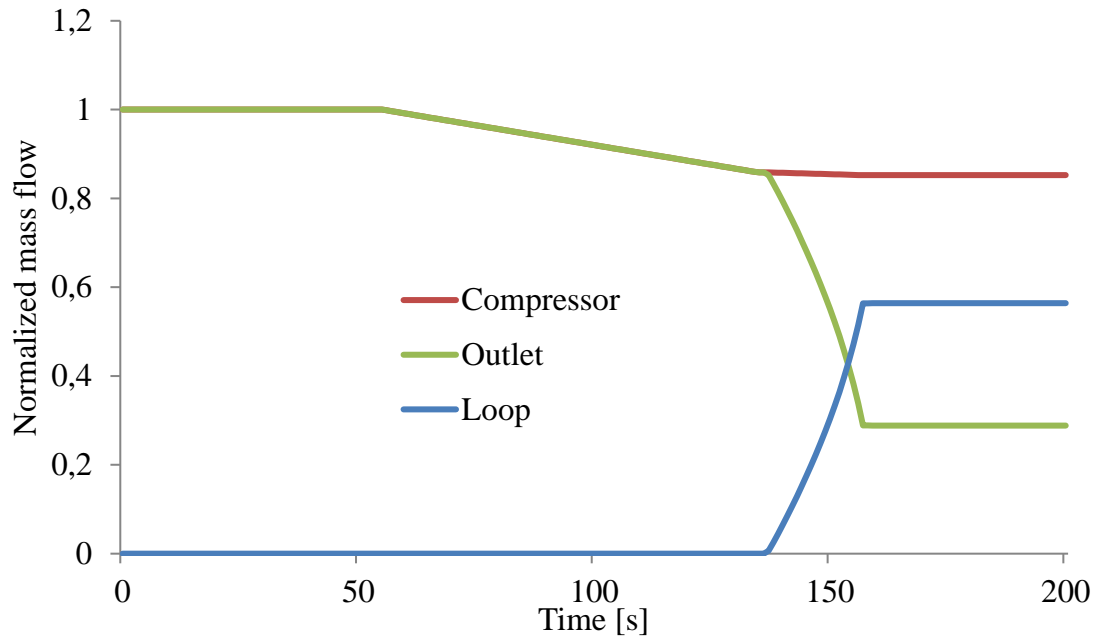
**Figure 4.8: The opening of the anti-surge valve during the steady state sequence.**



**Figure 4.9: The surge margin during the steady state sequence.**

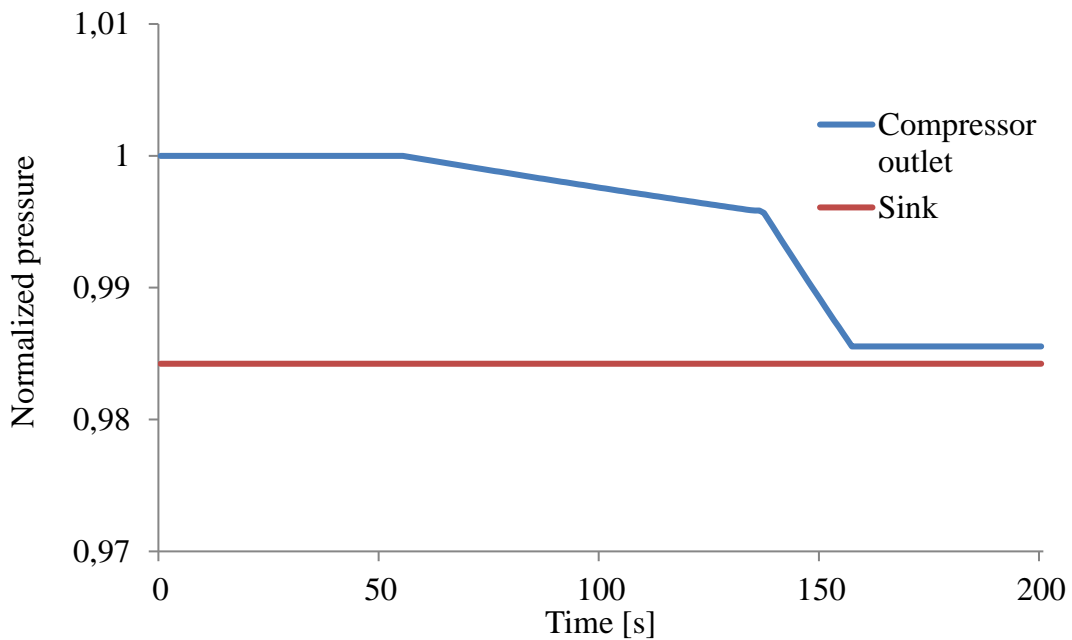
As the speed decreases the surge margin is decreasing as well. The surge margin is then kept at 10 % as can be seen in Figure 4.9 by the control system, as intended.

Figure 4.10 shows how the mass flow through the loop, the outlet and the compressor changes during the simulation. As can be seen in Figure 4.8 the valve starts to open which increases the mass flow through the loop and decreases the mass flow through the outlet of the system in order to keep the compressor mass flow constant, thus avoiding surge.



**Figure 4.10: The loop, outlet and compressor mass flow during the steady state sequence.**

Figure 4.11 shows how the pressure decreases during the simulation. It can be seen that as the valve opens the negative slope is increased, until the opening level is stable. The compressor outlet pressure still being above the sink pressure corresponds to the fact that mass flow still leaves the system.



**Figure 4.11: The outlet and sink pressure during the steady state sequence.**

## 4.2 Verification of the compressor train

To verify that the compressor train behaved as expected and with accuracy, both during start-up and steady state operation, the Dymola compressor train model was verified in three steps. First the chosen parameters was plotted individually for two different cases, in order to see how the model responded and thereby be able to tune the model to act as intended for more than one case. Then the operating line was plotted in two compressor maps and lastly the results were compared with measured data from the sites Port Said and Eischleben.

Even if the MD control system is based upon the control system for PG many modifications have been made. To get the controllers to behave as intended some parameter values had to be changed, for example the parameters  $k$ ,  $Ti$  and  $Td$  (all mentioned in [2.13.2 PID-controller](#)).

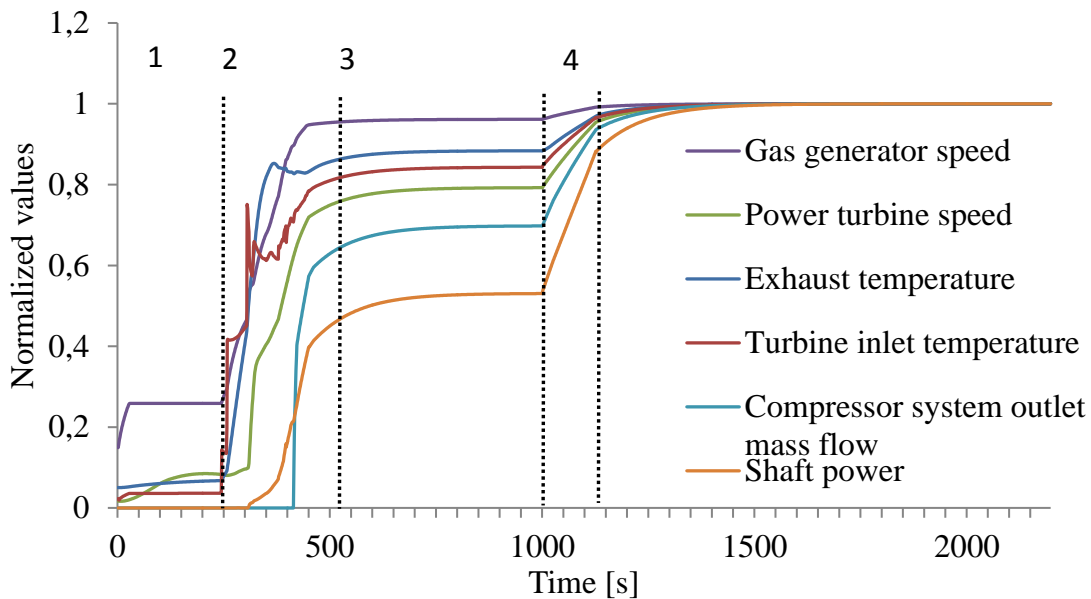
### 4.2.1 Individual plots

Table [4.3](#) shows the two simulated cases that the compressor train model was verified with. The cases correspond to the two chosen scenarios (1A 2023 and 1A 2024) from the data sheets given by the manufacturer.

**Table 4.3: Verification cases for compressor train. Case 1 corresponds to scenario 1A 2023 with a positive mass flow ramp and case 2 corresponds to scenario 1A 2024.**

| Case | $p_{comp. inlet}$<br>[psiA] | $p_{comp. outlet}$<br>[psiA] | $\dot{m}_{set point}$<br>[kg s <sup>-1</sup> ] | $\dot{m}_{ramp}$<br>[kg s <sup>-1</sup> ] | $J_{comp}$<br>[kg m <sup>2</sup> ] |
|------|-----------------------------|------------------------------|--|---|------------------------------------|
| 1    | 733.7                       | 1025.2                       | 231.29   | 100                                       | 100                                |
| 2    | 799.4                       | 1131.5                       | 269.57   | ''  | ''                                 |

In Figure 4.12 the results for case 1 can be seen. This plot covers the time span from start to 2200 s. By looking at the graph the general behaviour can be analysed. Sequence 1 represents the purge until ignition occurs at 2. This starts a fuel ramp that accelerates the system until the curves flatten at point 3, where operation speed is reached. In sequence 4 the mass flow set point is ramped and accelerates the system to its final level.



**Figure 4.12: Simulation results for Case 1, 2200 s. The numbers represent sequences mentioned in the text.**

To be able to analyse the start-up sequence Figure 4.13 is a close-up at a time span from 0 to 600 s for case 1. Here it can be seen that the power turbine has a small acceleration during purge. After ignition the turbine inlet and exhaust temperature start to rise. When the gas generator has reached a certain speed and the turbine inlet temperature is high enough, the power turbine starts to accelerate. Due to this the shaft power increases.

As showed in chapter 4.1 [Verification of the compressor system](#), the compressor needs to reach a certain rotational speed before the mass flow out of the compressor system increases.

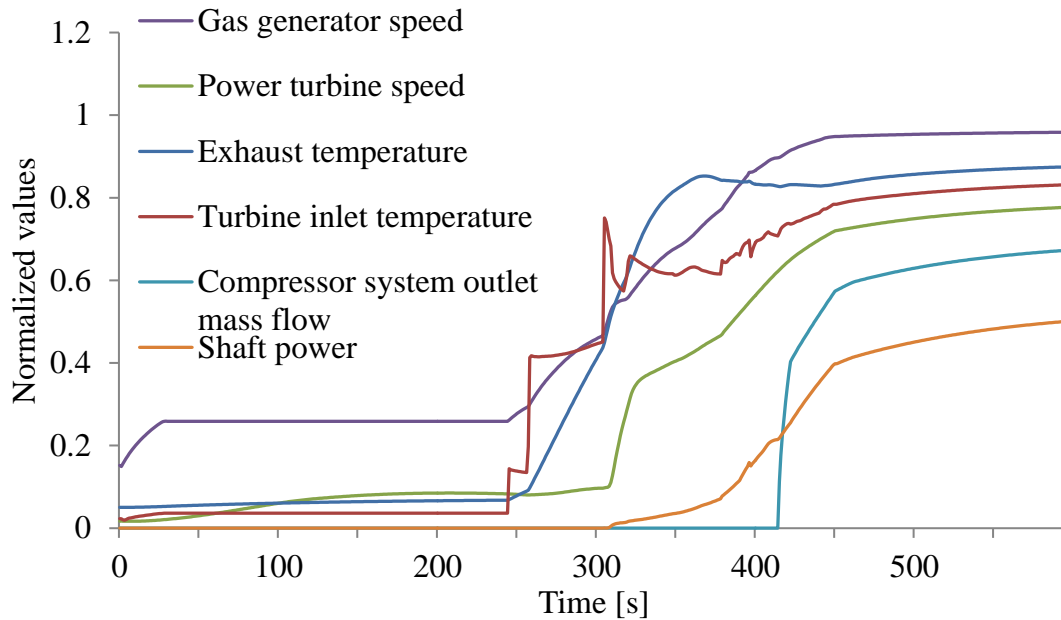


**Figure 4.13: Simulation results for Case 1, 600 s**

Figure 4.14 shows which controller is active during the simulation. The PAC interferes with the STC operation when the acceleration of the PT is too high just after ignition of the gas turbine has occurred. When the acceleration rate is below the limit the PAC deactivates and the STC activates again. As the GG speed of 6000 is reached the NGGL controls the acceleration of the GG until the SC takes over operation when the PT reaches min. continuous speed, 2745 rpm. The behaviour of the control system is steady with no rapid changes between different controllers.

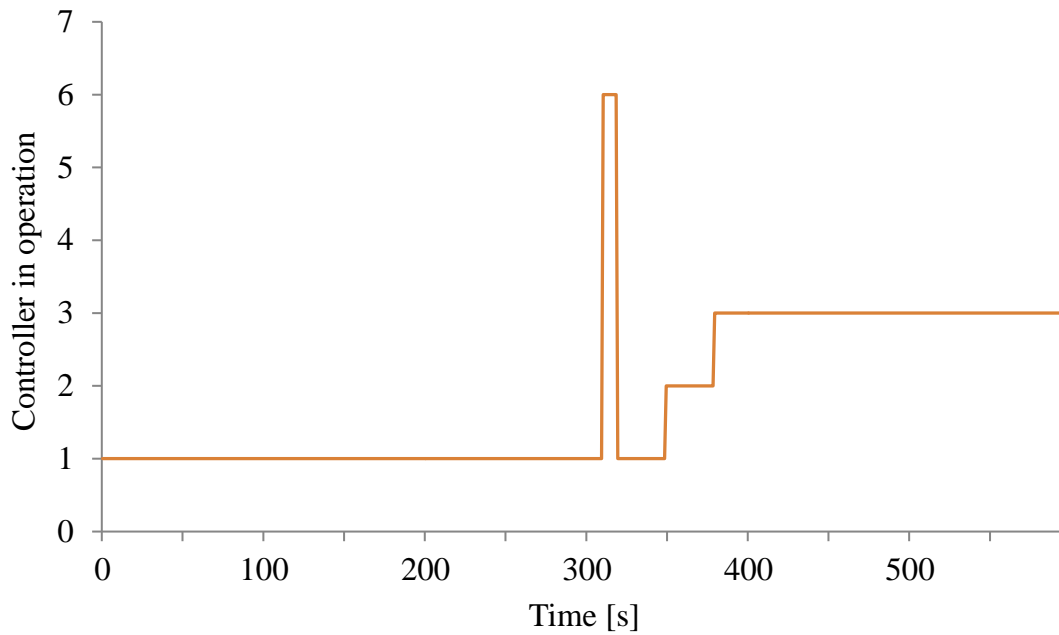


**Figure 4.14: Simulation results for Case 1, 600 s, showing which controller is active at a certain time. 1 indicates STC, 2 NGGL, 3 STC, 4 T0800L, 5 LLD and 6 the PAC.**

Figure 4.15 shows case 2 which has a higher mass flow set point. It also has higher inlet and outlet pressure, corresponding to scenario 1A 2024. This gives a higher speed for both the gas generator and the power turbine. The behaviour is more unstable compared to case 1, which is most obvious for the TIT. The acceleration of the PT differs also as it can not be clearly divided into three sections as for case 1. For case 1 three different slopes can be spotted, one for the STC, one for the NGGL and one for the SC between 300 and 450 seconds.

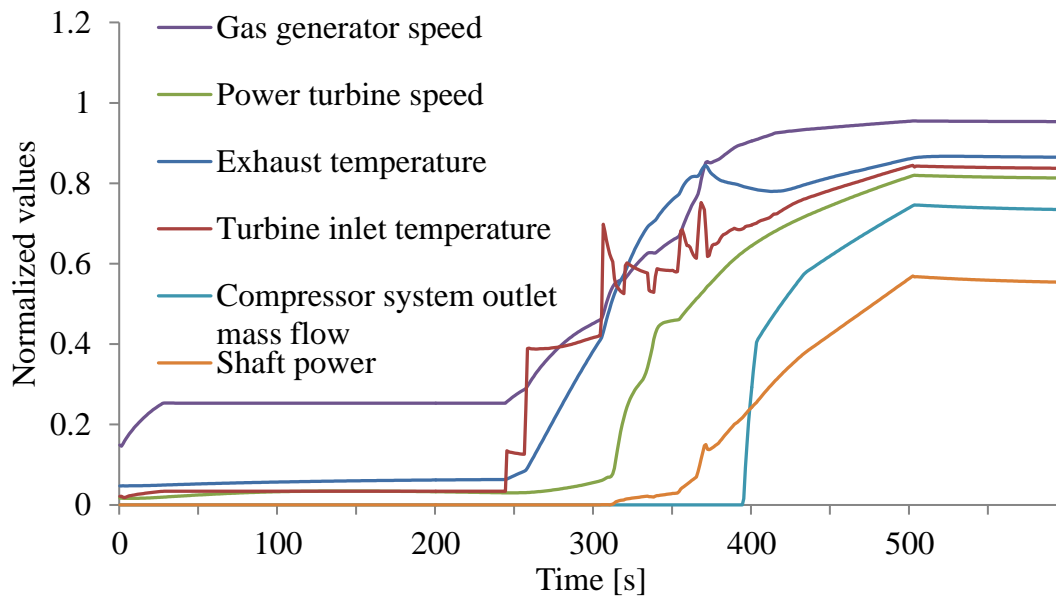
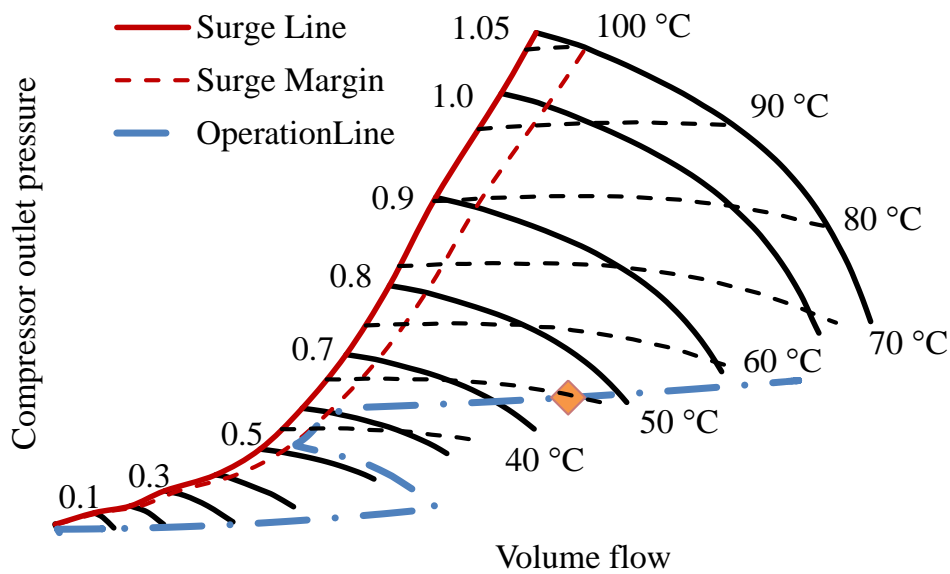


Figure 4.15: Simulation results for Case 2, 600 s

## 4.2.2 Compressor maps

To analyse how the simulation is performed with respect to the compressor maps the operation line is plotted in them. Figure 4.16 shows the operation line in the compressor map for scenario 1A 2023 and Figure 4.17 for scenario 1A 2024. In both cases it can be seen that the operation line has a great distance to the surge line during the first part of the start-up, when the graph is almost horizontal. As described in chapter 4.1 [Verification of the compressor system](#), the surge margin decreases when the anti-surge valve closes. In these figures this is visualized by the operation line moving closer to the dotted red surge margin line. When surge margin increases the operation line is moved away from the surge line again. After reached the (orange) operation point the mass flow (and speed) ramp takes the graph further to the right.





**Figure 4.16:** Compressor map for case 1 with blue operation line added. The solid black lines are speed lines and the dotted black lines represent the discharge temperature. The orange dot represents the operation point for the chosen scenario.

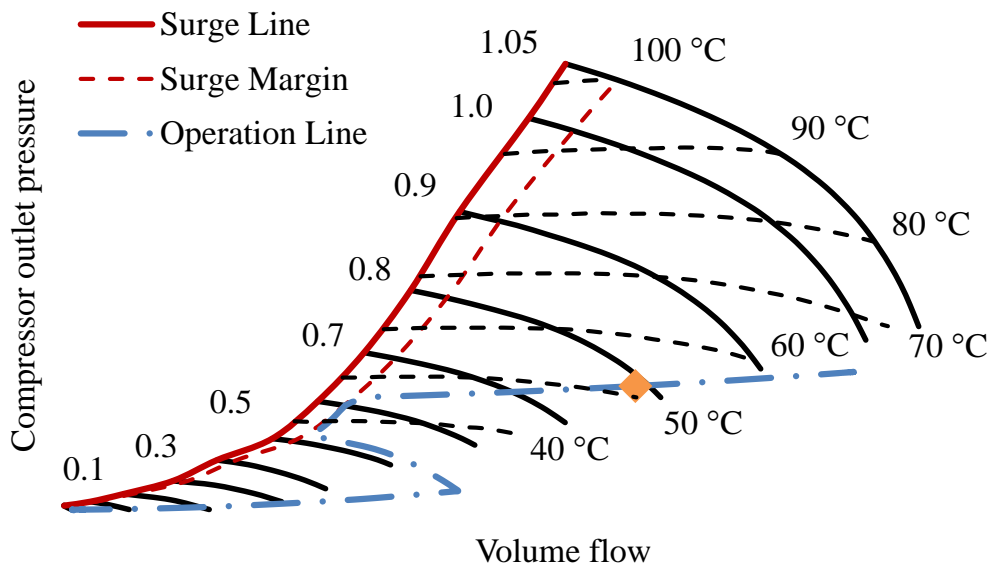


**Figure 4.17:** Compressor map for case 2 with blue operation line added. The solid black lines are speed lines and the dotted black lines represent the discharge temperature. The orange dot represents the operation point for the chosen scenario.

### 4.2.3 Site verification

STA-RMS was used to find data from MD sites with the SGT-700 as the driving source. The reason of using data from the SGT-700 is simply that there were yet no data available for the SGT-750 in MD applications and therefore the SGT-700 was used as the best alternative. Two sites were used in the verification process, Port Said in Egypt and Eischleben in Germany.

The goal of the verification was to compare the GG and PT rotational speeds. Though, it was not focused on the parameter values due to the fact that two different gas turbine models were compared, but more on the shape of the plots. Therefore the verification of the compressor train can be said to be a way to establish guidelines for the model and not something that had to agree entirely.

Figure 4.18 shows the rotational speeds from the simulation and from the site Eischleben, Germany. The red graphs, which show the gas generator speeds, have great similarity, which indicates accuracy of the model. Even if the actual speeds may not be equal, these normalized values are almost equal. The black graphs, which represent the power turbine speeds, have a larger deviation. This deviation is due to mechanical variations between the model and the machine on site. It is not sure that the driven component is the same as in the simulation, and there are many physical parameters that affect this start-up behaviour, such as inlet pressure, outlet pressure and mass flow for the driven compressor. By extension the gas turbine start sequence is strongly dependent on the start sequence of the driven compressor.

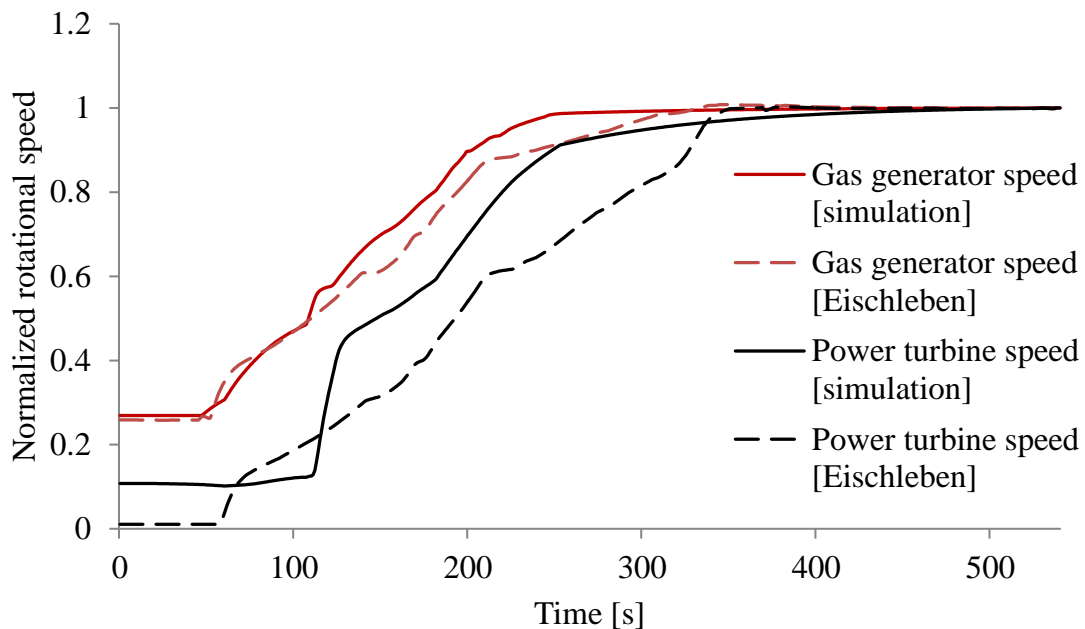


**Figure 4.18: Gas generator speed and power turbine speed from simulation results and from site Eischleben.**

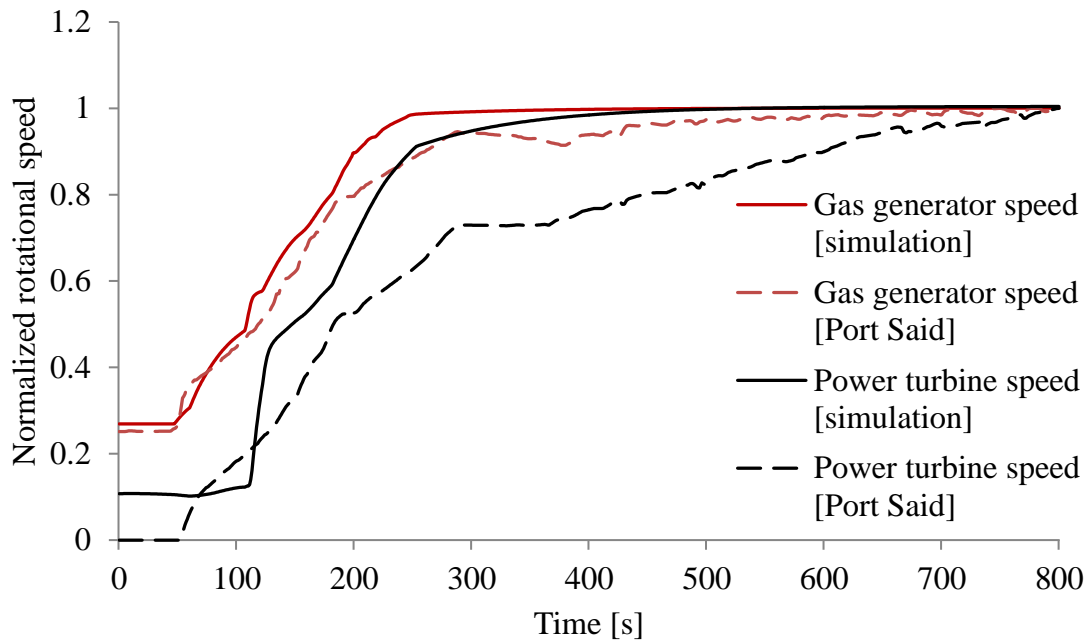


**Figure 4.19: Gas generator speed and power turbine speed from simulation results and from site Port Said.**

In Figure 4.19 the same comparison is done with data from site Port Said, Egypt. Just as for the comparison with Eischleben, the simulated gas generator speed follows the measured data well. The deviation for the power turbine speed is larger, and the same reasoning can be taken in this case as for Eischleben.



# 5. Behaviour analysis

When the model was verified and considered to correspond to reality it could be used to analyse how the gas turbine behaviour responds to changes of controller parameters. By running simulations with various values of interesting control system parameters it was possible to see how they affect the gas turbine behaviour. The chosen parameters were the fuel ramp in the STC, rotational inertia for the driven component, deactivation of the PAC and gas generator acceleration in NGGL. The simulations are presented in the following paragraphs. The controllers were described under [3.3 Dymola model of gas turbine control system](#).

**Table 5.1: The cases that were simulated to study how the parameters affect the gas turbine behaviour.**

| Case | Original case | Changed parameter                                    | Figure to compare with |
|------|---------------|--|------------------------|
| a)   | 2             | STC <sub>fuel ramp</sub> increased                   | <a href="#">4.15</a>   |
| b)   | 1             | Rotational inertia increased                         | <a href="#">4.13</a>   |
| c)   | 1             | PAC deactivated                                      | <a href="#">4.13</a>   |
| d)   | 1             | NGGL <sub>gas generator acceleration</sub> decreased | <a href="#">4.13</a>   |

## 5.1 Fuel ramp in STC - a)

To see how the gas turbine behaviour is affected by the fuel ramp in the STC, the model is simulated with different values of the fuel ramp. Figure [5.1](#) shows the behaviour with a steeper ramp, the value recommended by [\[24\]](#), which is higher than in the other simulated cases.

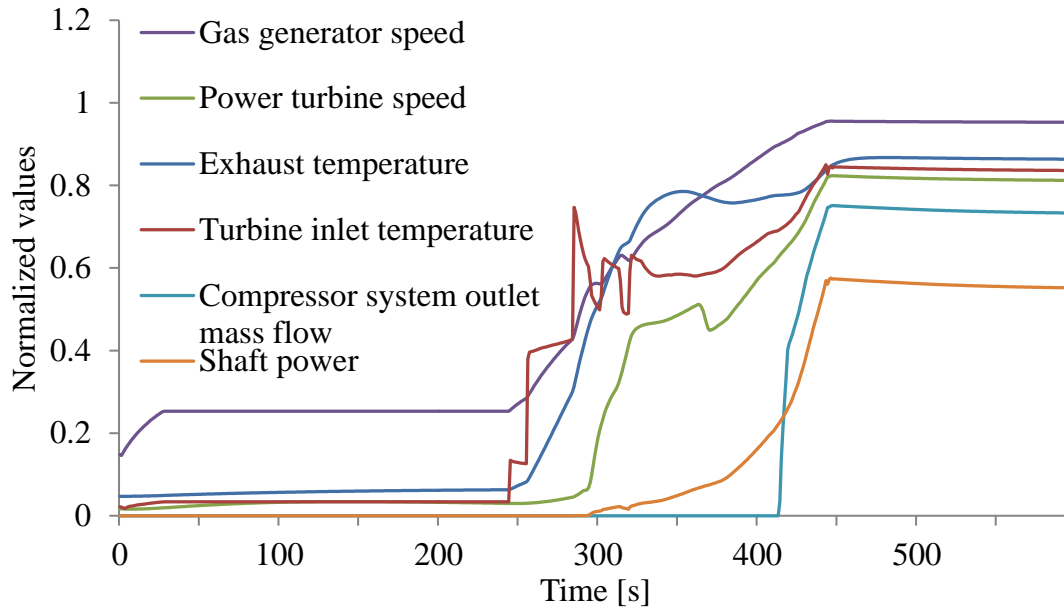


**Figure 5.1: Simulation results for Case a)**

As the Figure 5.1 shows, the higher fuel ramp causes an instability that cannot be seen in the other cases. The instability can clearly be seen on the acceleration of the power turbine during start-up (300-400 s). Also the graphs for turbine inlet temperature, shaft power and mass flow become more unsteady than for the other cases. The TIT can clearly be seen to be unsteady while the power and mass flow are harder to notice.

Figure 5.2 shows the GG and PT speeds for case a) and case 2. As can be seen there is difference in both GG and PT acceleration. The higher acceleration of the GG in case a) is, logically, caused by the higher fuel ramp. This causes a higher PT acceleration which gives instability when STC is deactivated.

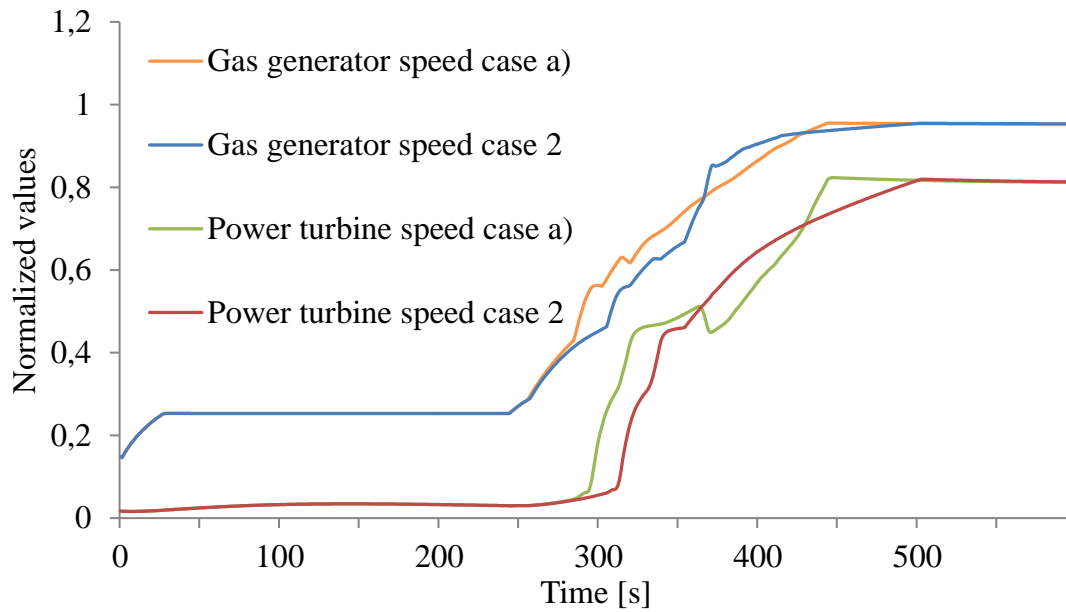


**Figure 5.2: Rotational speeds for case 2 and case a)**

## 5.2 Rotational inertia - b)

Depending on what type of component the gas turbine drives, the rotational inertia varies. A higher inertia affect the acceleration of the component, and because the component is directly connected to the PT, it affects the PT acceleration as well. Figure 5.3 shows case b), where this phenomena can be studied. It can be seen that the general behaviour is similar to case 1, both during start-up and when ramping the mass flow set point.

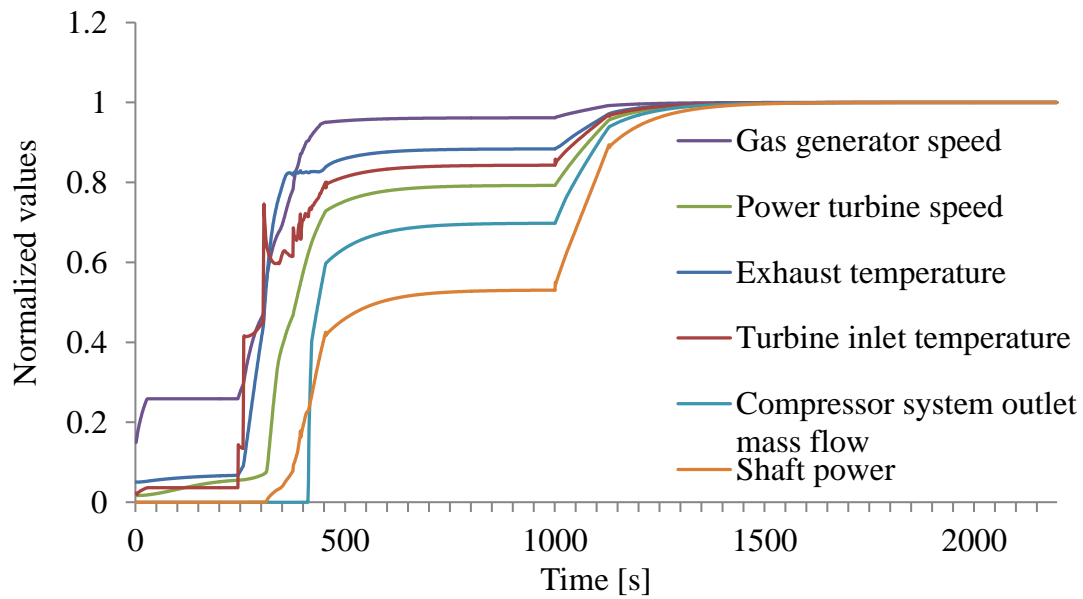


**Figure 5.3: Simulation results for Case b)**

Figure 5.4 shows case b), the same case as Figure 5.3 but with a zoomed view. One effect of the higher inertia is that the power turbine has a slower acceleration in the beginning, both during purge and just after ignition. Though it accelerates faster in the end of the start-up due to its higher inertia and experiences a bit of an overshoot of the set value. This can also be seen in Figure 5.5, which shows the GG and PT speed for case b) and case 1.



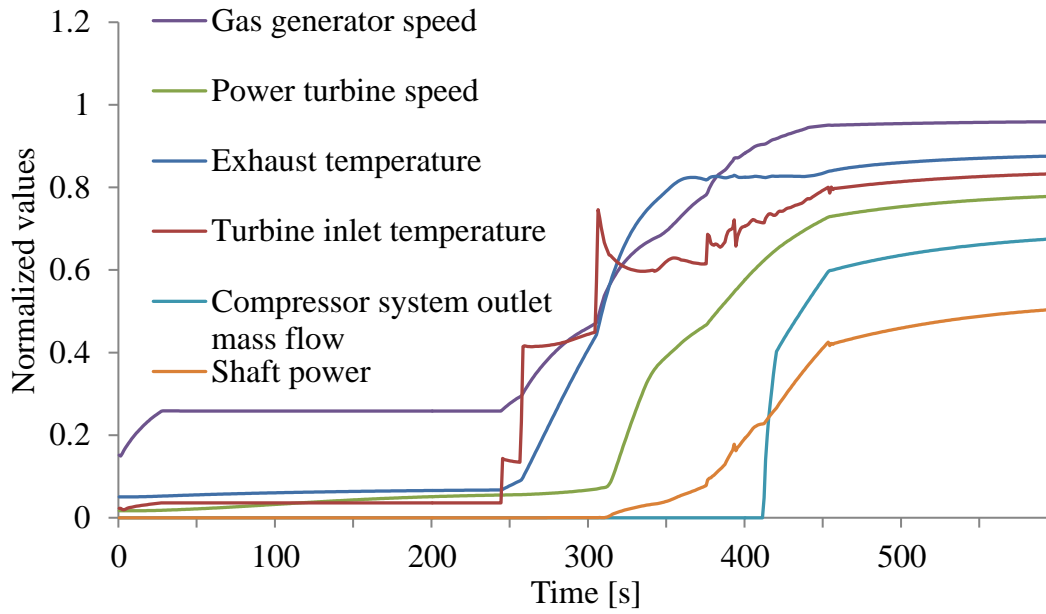


Figure 5.4: Simulation results for Case b), 600 s

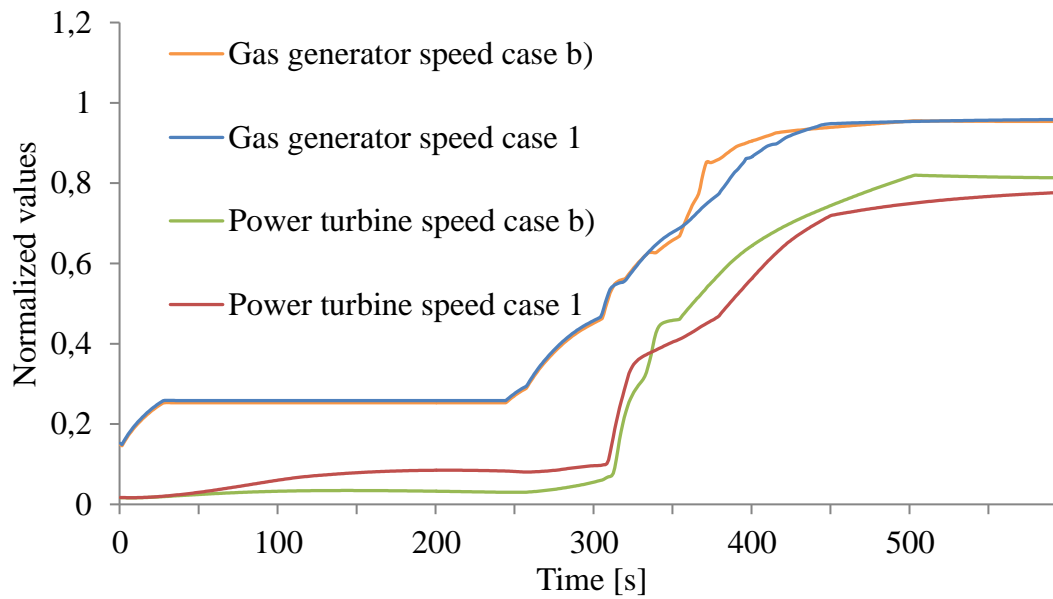
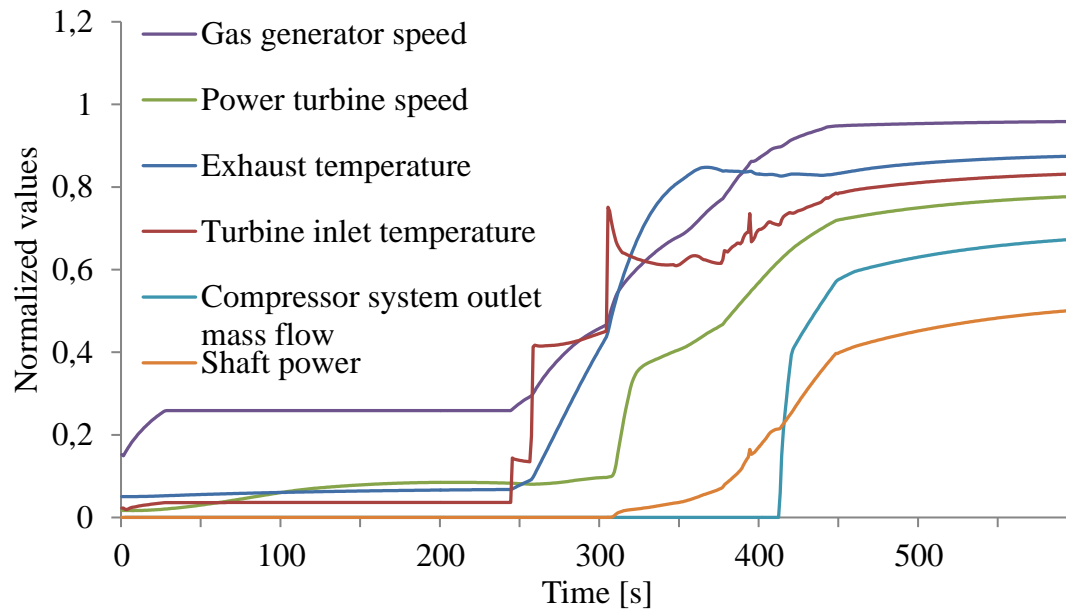


Figure 5.5: Rotational speeds for case 1 and case b)

### 5.3 Deactivation of PAC - c)

As described in section 3.3 [Dymola model of gas turbine control system](#), the PAC controls the acceleration of the power turbine. Figure 5.6 shows a simulation with the PAC inactive.



**Figure 5.6: Simulation results for Case c)**

In the figure that shows case c) it can be hard to compare the deviations between case 1 (active PAC) and case c) (inactive PAC). For that reason Figure 5.7 shows a comparison between the rotational speeds in the two cases. Even if the deviation is barely viewable this indicates that the PAC does affect the start-up sequence. The reason to why they differ during such a small interval is that it is only during this time the PAC is active. As the figure shows the PAC lowers the acceleration slightly in this interval, as intended. The TIT is also seen to be more steady when the PAC is deactivated.

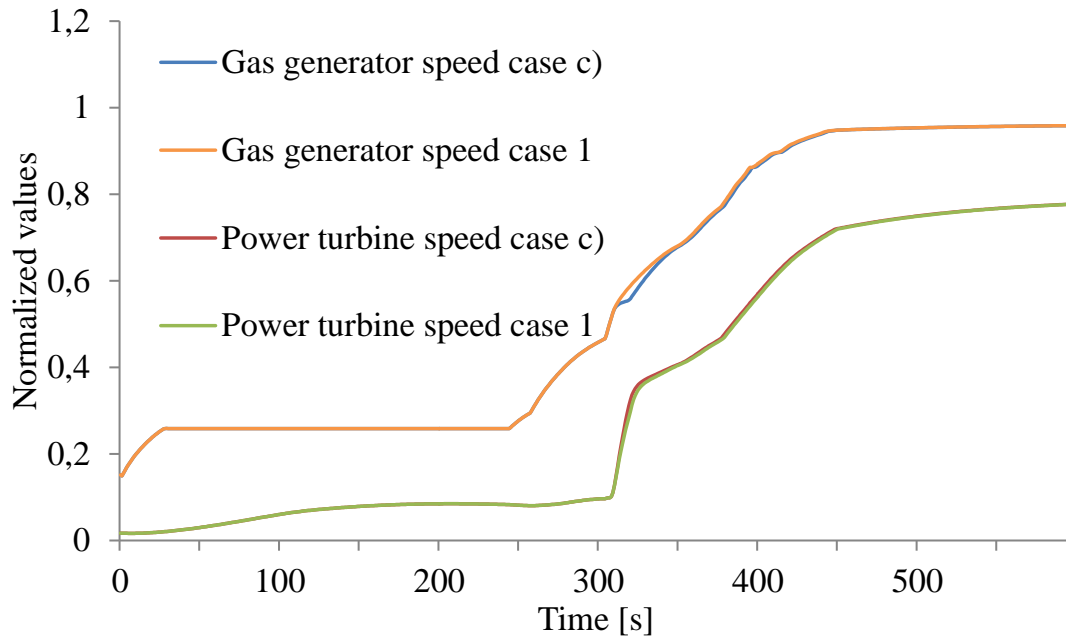
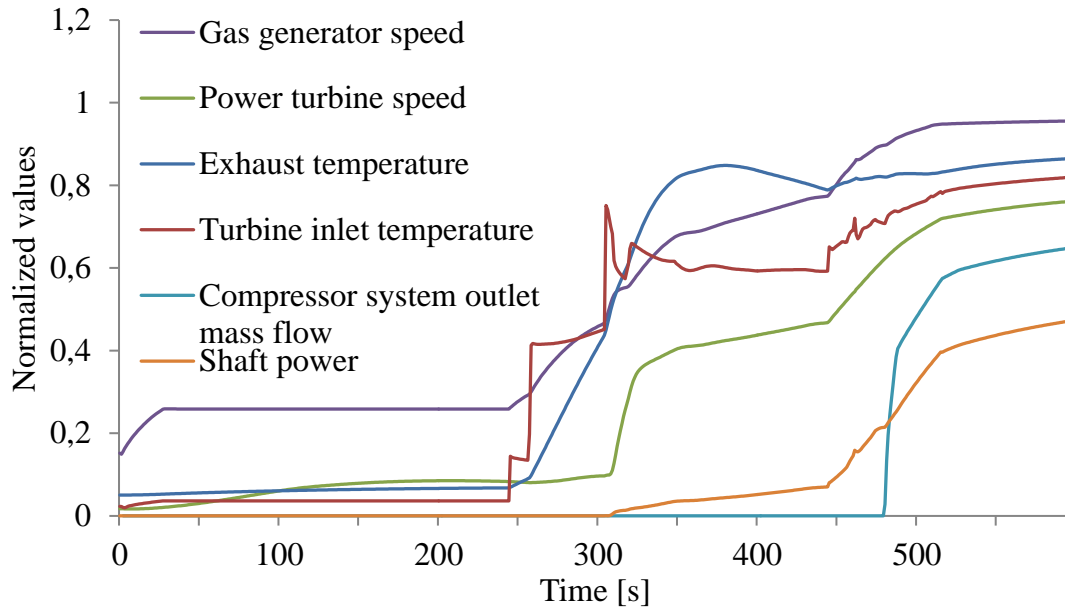


Figure 5.7: Rotational speeds for case 1 and case c)

#### 5.4 Gas generator acceleration in NGGL - d)

As described in section [3.3 Dymola model of gas turbine control system](#), the NGGL controls the acceleration of the gas generator. In this case the limit of this acceleration is decreased. This gives a slower acceleration for the gas generator during the time when NGGL is active, at around 350 to 450 s. The simulation results can be seen in Figure [5.8](#).



**Figure 5.8: Simulation results for Case d)**

Figure 5.9 shows a comparison between case d) and 1. This figure shows clearly how the gas generator acceleration differ between the cases. This causes the same difference for the power turbine, as also can be seen in the figure.

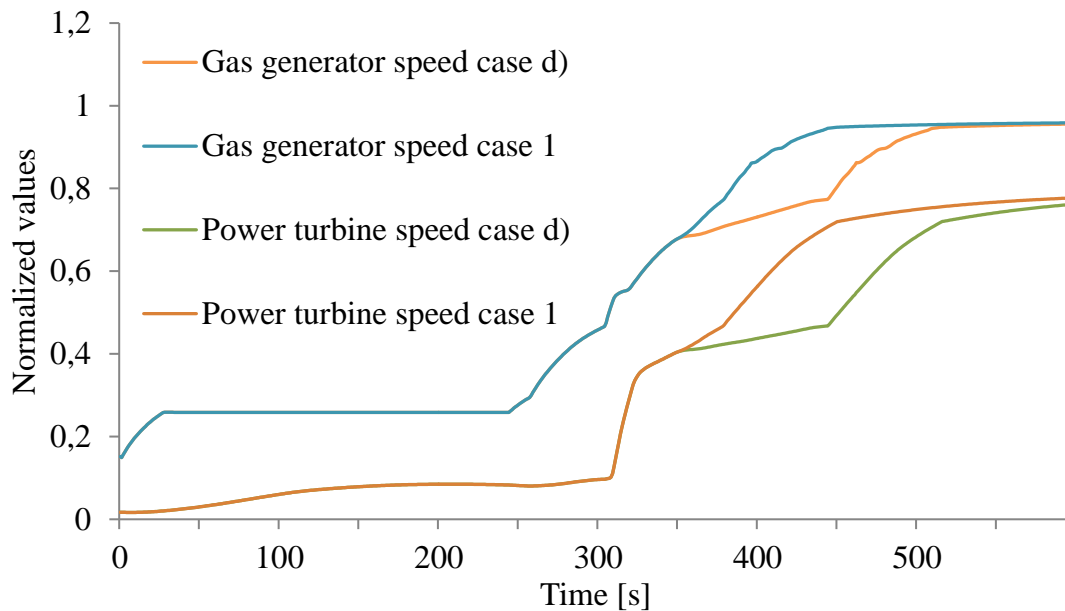


**Figure 5.9: Simulation results for Case 1 and case d)**

# 6. Discussion

The objective of this project was to design a model in Dymola that corresponds to reality and can be used in future work. The verification determined how large and what kind of deviations there were between reality and the model. In this section these deviations and relationships are discussed.

## 6.1 Compressor model

The design of the compressor maps used as input caused inaccuracy for some parameters. Firstly, they have a limited range of speeds, why they had to be extended for speeds under 50 %. To make the compressor model more accurate and complete it would be advantageous to use maps with a wider range of speeds. Secondly, the discharge temperature scale in the compressor maps causes deviations. Because it had to be manually read and put into the model there is an uncertainty of the temperature output and hence the polytropic efficiency. In this model it has been done as good as possible, according to the authors, but for future use a change of the compressor map design or format would make it easier to add the data in the model and thereby make the output from the compressor maps more accurate.

As mentioned in [3.2.3 Compressibility](#), the compressibility factor is included in the model, though, it has to be manually added in two different locations which is not favourable. The compressibility factor should be computed by Dymola instead to get the right density and inner energy.

## 6.2 Compressor train

The compressor train can be seen as a general model that can be used as a basic model to represent different compressors, connected to a gas turbine. The aim was to agree as much as possible with the site El Encino, Mexico, where the general design originates from. This does not mean that all parameters are tuned after this site. Many parameters

of for example the PID-controllers, has been chosen to fit this model specifically. To make the model more reliable more time has to be spent on various components. As mentioned in [1.3 Limitations](#), focus has been to study the gas turbine behaviour, not specific parameter values.

The control system of the gas turbine was carefully modified, to have the ability to use the same control system in different applications. For example it is possible for the user to either choose PG or MD mode, and still use the same control system. Despite this, small changes had to be done in the gas turbine using this control system. This is not optimal but the changes were necessary to be able to run the system in a MD mode.

## 6.3 Verification

### 6.3.1 Compressor system

When modelling the compressor system some limitations in Dymola were discovered that makes the thermodynamic calculations inaccurate. As mentioned in [4.1 Verification of the compressor system](#), the enthalpy functions are not thermodynamically correct. Dymola calculates the enthalpy only with respect to temperature, which is a reasonable approximation when calculating performance of a gas turbine. In this project however, the compressor inlet pressure is somewhere in the region of 50 bar instead of one bar which then causes the model to behave inaccurate. The result of this was a low accuracy of the compressor power, which affects the shaft power of the gas turbine. To solve this problem major programming modifications needs to be done in Dymola, an objective too big to include in this project. This is not a major problem though, because the purpose of the project was not to have exact values but to verify the behaviour of the system, which can be seen as accomplished. Due to the fact that the gas turbine only operates in regions far from critical regions it can be assumed that the enthalpy difference does not affect the gas turbine behaviour.

The other verification parameters of the compressor system were in a reasonable range, according to the authors, when considering the limitations of the project. They differ less than 3 % which is acceptable as the temperature of the maps were difficult to implement in the model.

The verification of the compressor system was also about verifying the function of the anti-surge loop for the two cases. As illustrated in the previous chapter the surge margin is kept at 10 % by the anti-surge control system and the opening and closing of the anti-surge valve follows the prescribed times according to [21]. Since no data for the driven unit could be found the behaviour of the compressor system was hard to tune in, in order to reflect reality and no further verification was performed.

### 6.3.2 Compressor train

The compressor train model is acting in a logical manner when analysing the figures in the previous chapter. It serves its purpose as a model for the MD application with an SGT-750.

The activation of the different controllers can be seen in Figure 4.14. There are no unnecessary changes between the controllers which makes the model fast and stable. Of course there could be improvement in the different set points of the controllers to get an even smoother transition between them. As can be seen in Figure 4.13 the TIT experiences a quite unsteady behaviour, which could be dampened with tuning of the controllers. Though the TIT in reality never experiences these kinds of fluctuations because of system inertia, but in the model the temperature is calculated and therefore behaves in such an unstable manner. The controllers also fulfil their purpose of keeping different critical parameters at, or above, their limits and the compressor train is therefore never in any danger of entering surge or being accelerated too quickly during start-up.

Case 2 shows that the model can handle different inlet pressures in the compressor system, which is a case important for the validity of the model since the circumstances of the pipeline, i.e. the inlet conditions of the compressor system changes over time.

### 6.3.3 Compressor maps

The compressor maps, Figure 4.16 and 4.17, show the operation line of case 1 and 3. In both cases the surge margin is decreased to the surge limit during start-up, this is done to build up pressure in the driven compressor. It is unclear if that is the common way during start-up or if the valve is closed differently in order to keep a greater distance to the surge limit. Since no measured data could be found for the surge margin, no further tuning of the anti-surge valve was performed.

### 6.3.4 Eischleben and Port Said

As mentioned the machines compared were not the same and differs in their behaviour and performance so the shape of the curves were of more interest. The acceleration of the GG is similar to both sites while the PT speed differs more. A reason for this is of course the fact that they are driving different compressors with different characteristics and that the whole compressor train differs. Another reason could be the fact that the engine control differs between the machines. Different fuel ramps and different set points for the different controllers contribute to the difference. The simulated PT speed starts from a higher speed than both Eischleben and Port Said which could be caused by the inaccuracy of the compressor and PT maps at speeds below 50 % of nominal speed.

Also the model is not able to start at too low speeds which is why there is a higher speed of the PT before ignition.

The start time of the simulation differs a bit from the start time of Port Said. Port Said reaches its operating speed at approximately 800 seconds while the simulation reaches it at 500 seconds. This could be caused by different values of the controller parameters or that they are different compressor trains as mentioned before. Though the start time of Eischleben is quite similar to the simulation which indicates that the start time can vary from machine to machine and that the model starts within a reasonable time space.

### **6.3.5 Behaviour analysis**

The higher fuel ramp in case a) is seen to give a more unstable variation of the TIT, an uneven acceleration of the power turbine and a more unstable control of the system which can be seen in Figure 5.1. This might be an indication that a lower fuel ramp could be advantageous during start-up for a compressor train with the SGT-750.

As the inertia was increased in case b) the model behaves in a similar way, but with slightly smaller transients which is what could be expected as the system gets slower in reacting to changes.

Case c), where the PAC is deactivated the behaviour of the TIT is more stable than when the PAC is active. The unsteady behaviour is caused when the PAC decreases the temperature and the STC is activated once again and increases it, as can be seen in Figure 4.14. The simulations indicates that the PAC in this case has a small impact on the GG and PT speed acceleration. If so, the benefit of having the PAC can be questioned. A deactivation gives a more stable and faster simulation but it is important to note that the PAC may be necessary for other cases, depending on inertia and other physical limitations of the machine. For a machine with low inertia it would probably be necessary with an active PAC.

When changing the ramp of the NGGL in case d) the acceleration is of course slower during start-up and gives a slower starting of the compressor train. Except for that there are small differences from case 1 and the time is the main parameter affected due to this change.



# 7. Conclusions

- The objectives of the project was to create a model that corresponds to reality and can be connected to a gas turbine model. The verification shows that the compressor system serves this purpose when connected to the gas turbine. The authors consider that the existing deviations is within approved area to regard it as a reliable compressor train model considering the limitations.
- As mentioned under [1.3 Limitations](#), the focus has been on analysing the behaviour of the gas turbine and only model the parts that affect the running of either the gas turbine or the compressor system. Thus, if the model is to be used for analysing specific parameter values, the system components can be tuned in for that specific case.
- The gas turbine control system is made as general as possible which makes it applicable to different gas turbines and applications, both for PG and MD.
- The behaviour analysis shows that the lower fuel ramp affects the compressor train in a positive manner for the simulated cases. It also shows that a deactivation of the PAC affects the compressor train in a positive manner for these specific cases. This indicates that the PAC might be redundant, but for other cases with different inertia and physical behaviour it might be necessary to have a PAC. The ramp of the NGGL mainly affects the starting time and if a fast start is desired it should be as high as possible.
- With this model it is now possible to study how the gas turbine design can be optimized for a MD application.



## 8. Future work

To further develop this project the following action points are suggested:

- Improve the medium handling in Dymola. To ensure correct enthalpy the functions should be modified to handle real gases where the enthalpy depends on both temperature and pressure.
- Add the compressibility factor in Dymola. The compressibility factor is in this project handled as a user input, where the user has to set the value in two different locations. This is not optimal and as future work the factor should be implemented into the functions of the model and thereby be generated by Dymola.
- Simulate more scenarios. To make sure the model can handle a wide range of pressures, mass flows and speeds more cases can be done. To be able to do this in a correct way more compressor maps should be implemented into the model. This action needs digitalized compressor maps that easily can be used as input.
- Simulate larger systems. Considering the fact that many sites consist of several compressor trains it would be interesting to simulate this in Dymola. Connecting compressor train models makes it possible to predict performance parameters for a whole compressor site.



## 9. References

- [1] Kulturarv-Östergötland. Finspång. [http://www.kulturarvostergotland.se/img/html\\_pobfin/html/finsp\\_indhi.html](http://www.kulturarvostergotland.se/img/html_pobfin/html/finsp_indhi.html), 2003. Accessed: 2017-02-01.
- [2] Kulturarv-Östergötland. Asea-stal. <http://web.archive.org/web/20080207010024/http://www.808multimedia.com/winnt/kernel.htm>, 2003. Accessed: 2017-02-01.
- [3] Rainer Kurz and Klaus Brun. Site performance test evaluation for gas turbine and electric motor driven compressors, 2005.
- [4] Meherwan P. Boyce. *Gas Turbine Engineering Handbook*. Gulf Professional Publishing, third edition, 2006.
- [5] R. L. Casper and R. E. Spector. The Im6000 gas turbine as a mechanical drive power source. *GE Marine & Industrial Engines, General Electric Company*, 1992.
- [6] P. E. Garrison T. E. Ekstrom. Gas turbines for mechanical drive applications. [https://powergen.gepower.com/content/dam/gepower-pgdp/global/en\\_US/documents/technical/ger/ger-3701b-gas-turbines-mechanical-drive-applications.pdf](https://powergen.gepower.com/content/dam/gepower-pgdp/global/en_US/documents/technical/ger/ger-3701b-gas-turbines-mechanical-drive-applications.pdf). Accessed: 2017-04-06.
- [7] Vivek Bhardwaj. Rotary compressors and types | working principle | engineering explained. <http://aermech.com/rotary-compressors-and-typesworking-principleengineering-explained>, 2015. Accessed: 2017-03-13.
- [8] Peyman J. Positive displacement compressors: Reciprocating compressor. <http://scopewe.com/positive-displacement-compressors-reciprocating-compressor/>, 2013. Accessed: 2017-03-13.
- [9] H. Saravanamuttoo, G. Rogers, H. Cohen, and PV. Straznicky. *Gas Turbine Theory*. Pearson Education Ltd, sixth edition, 2009.

- 
- [10] Mecholic. Centrifugal compressor schematic diagram. <http://www.mecholic.com/2016/07/centrifugal-compressor-parts-pressure-velocity-variation-curve.html>, 2016. Accessed: 2017-03-13.
- [11] Michael A. Boles Yunus A. Çengel. *Thermodynamics - An Engineering Approach*. McGraw-Hill, sixth edition, 2007.
- [12] Frank Kreith. *Mechanical Engineering Handbook*. CRC Press LLC, first edition, 1999.
- [13] S.L. Dixon. *Fluid Mechanics, Thermodynamics of Turbomachinery*. Butterworth-Heinemann, fourth edition, 1998.
- [14] A.M.Y Razak. *Industrial gas turbines - Performance and operability*. Woodhead Publishing Limited, first edition, 2007.
- [15] E. M. Greitzer. Review - axial compressor stall phenomena. *Journal of Fluids Engineering*, 102:134–136, 6 1980.
- [16] E. M. Greitzer. Surge and rotating stall in axial flow compressors. *Journal of Engineering for Power*, pages 190–191, 1976.
- [17] Christer von Wowern. *PM about calculating polytropic efficiency with sT-method*. Siemens Internal, 2012.
- [18] Anna Sjunnesson. Interview. 4 2017.
- [19] Bengt Sundén. *Värmeöverföring*. Studentlitteratur, Lund, 2006.
- [20] John H. Lienhard IV and John H. Lienhard V. *A Heat Transfer Textbook*. Phlogiston Press, Massachusetts, third edition, 2005.
- [21] Unknown. *A surge philosophy*. Siemens Internal, 2015.
- [22] Karl Åström and Tore Hägglund. *PID Controllers: Theory, Design, and Tuning*. Instrument Society of America, second edition, 1995.
- [23] PE David S. Moelling and Tetra Engineering Group Inc Peter S. Jackson, PE. Startup purge credit benefits combined cycle operations. <http://www.powermag.com/startup-purge-credit-benefits-combined-cycle-operations/>, 2012. Accessed: 2017-05-23.
- [24] Marie Kvilleng. *SGT-750 Engine Control Specification*. Siemens Industrial Turbomachinery, f edition, 2016.
- [25] Natural Gas Supply Association. Natural gas explained. [https://www.eia.gov/energyexplained/?page=natural\\_gas\\_home](https://www.eia.gov/energyexplained/?page=natural_gas_home), 2016. Accessed: 2017-03-14.

## 9. REFERENCES

---

- [26] Editor E.W. McAllister. *Pipeline, Rules of Thumb*. Gulf Professional Publishing, fifth edition, 2002.
- [27] Natural Gas Supply Association. The transportation of natural gas. <http://naturalgas.org/naturalgas/transport/>, 2013. Accessed: 2017-03-14.
- [28] Siemens AG. Gas turbine sgt-750. [http://www.energy.siemens.com/br/pool/hq/power-generation/gas-turbines/sgt-750/SGT-750\\_factsheet\\_en.pdf](http://www.energy.siemens.com/br/pool/hq/power-generation/gas-turbines/sgt-750/SGT-750_factsheet_en.pdf), 2016. Accessed: 2017-03-13.
- [29] Siemens AG. Single shaft vertical split turbocompressors. <http://www.energy.siemens.com/co/en/compression-expansion/product-lines/single-shaft-vertical-split/stc-sv.htm#content=Benefits>, 2017. Accessed: 2017-04-07.
- [30] Dassault Systems. Catia systems engineering - dymola. <https://www.3ds.com/products-services/catia/products/dymola>. Accessed: 2017-03-15.
- [31] Flow Phase Inc. Vleflash. <http://www.flowphase.com/Products/flash.html>. Accessed: 2017-05-22.
- [32] Bonnie J. McBride, Michael J. Zehe, and Sanford Gordon. Nasa glenn coefficients for calculating thermodynamic properties of individual species. <https://www.grc.nasa.gov/WWW/CEAWeb/TP-2002-211556.pdf>, 2002. Accessed: 2017-04-12.
- [33] Pumps & Systems. Swing check valve. <http://www.pumpsandsystems.com/images/stories/valves/val-maticfig1.jpg>. Accessed: 2017-03-14.
- [34] Alexandra Foley. How to model a shell and tube heat exchanger. <https://www.comsol.com/blogs/how-model-shell-and-tube-heat-exchanger/>, 2013. Accessed: 2017-03-14.
- [35] M.O. McLinden E.W. Lemmon and D.G. Friend. Thermophysical properties of fluid systems in nist chemistry webbook, nist standard reference database number 69, eds. p.j. linstrom and w.g. mallard, national institute of standards and technology, gaithersburg md, 20899, doi:10.18434/t4d303. Accessed: 2017-05-16.